MODE II FATIGUE CRACK GROWTH BEHAVIOR AND MODE II FRACTURE TOUGHNESS OF 7050 ALUMINUM ALLOY IN TWO ORIENTATIONS

A THESIS SUBMITTED TO
THE GRADUATE SCHOOL OF NATURAL AND APPLIED SCIENCES
OF
THE MIDDLE EAST TECHNICAL UNIVERSITY

BY

M.ENDER YURTOĞLU

IN PARTIAL FULLFILLMENT OF THE REQUIREMENTS
FOR
THE DEGREE OF MASTER OF SCIENCE
IN
METALLURGICAL AND MATERIALS ENGINEERING

JANUARY 2013

Approval of the thesis:

MODE II FATIGUE CRACK GROWTH BEHAVIOR AND MODE II FRACTURE TOUGHNESS OF 7050 ALUMINUM ALLOY IN TWO ORIENTATIONS

submitted by **M.ENDER YURTOĞLU** in partial fulfillment of the requirements for the degree of **Master of Science in Metallurgical and Materials Engineering Department, Middle East Technical University** by,

Prof.Dr. Canan Özgen _____
Dean, Graduate School of **Natural and Applied Sciences**

Prof.Dr. Hakan Gür _____
Head of Department, **Metallurgical and Materials Eng.**

Prof.Dr. Rıza Gürbüz _____
Supervisor, **Metallurgical and Materials Eng. Dept., METU**

Examining Committee Members:

Prof.Dr. Bilgehan Ögel
Metallurgical and Materials Eng. Dept., METU _____

Prof.Dr. Rıza Gürbüz
Metallurgical and Materials Eng. Dept., METU _____

Prof.Dr. Hakan Gür
Metallurgical and Materials Eng. Dept., METU _____

Prof.Dr. Cevdet Kaynak
Metallurgical and Materials Eng. Dept., METU _____

Assist.Prof.Dr. Kazım Tur
Metallurgical and Materials Eng. Dept., Atılım University _____

Date: _____

I hereby declare that all information in this document has been obtained and presented in accordance with academic rules and ethical conduct. I also declare that, as required by these rules and conduct, I have fully cited and referenced all material and results that are not original to this work.

Name, Last Name: M.Ender YURTOĞLU

Signature :

ABSTRACT

MODE II FATIGUE CRACK GROWTH BEHAVIOR AND MODE II FRACTURE TOUGHNESS OF 7050 ALUMINUM ALLOY IN TWO ORIENTATIONS

Yurtoğlu, M.Ender
M.S., Department of Metallurgical and Materials Engineering
Supervisor: Prof. Dr. Rıza GÜRBÜZ

February 2013, 58 Pages

Fatigue crack growth behavior of AA7050 T7451 aluminum alloy under mode II loading condition in two orientations was investigated. Compact shear specimens were prepared in TL and LT directions. A loading frame for mode II type of loading was manufactured. Using the loading frame and the specimen, K_{IIC} values and mode II fatigue crack growth rates were calculated.

Fractographic analysis of the fracture surfaces of both mode II fracture toughness test specimens and mode II fatigue crack growth test specimens were done to examine the effects of mode II load.

K_{IIC} values were measured between 1.3 and 1.5 times the K_{IC} values for this alloy. As for mode II fatigue crack growth rates, TL orientation shows the highest mode II fatigue crack growth resistance.

Keywords: AA7050, Mode II fatigue crack growth rate, mode II fracture toughness, shear loading, mode II loading.

öz

7050 ALÜMİNYUM ALAŞIMININ İKİ ORYANTASYONDA MOD II YORULMA ÇATLAK İLERLEME DAVRANIŞI VE MOD II KIRILMA TOKLUĞU

Yurtoğlu, M.Ender
Yüksek Lisans, Metalurji ve Malzeme Mühendisliği Bölümü
Tez Yöneticisi: Prof.Dr.Rıza Gürbüz

Şubat 2013, 58 Sayfa

AA7050 T7451 alüminyum alaşımının 2 oryantasyon için mod II yüklemesi altında yorulma çatlak ilerleme davranışı incelenmiştir. Kompakt kesme numuneleri LT ve TL yönlerinde hazırlanmıştır. Mod II tip yükleme için bir yükleme aparatı imal edilmiştir. Bu yükleme aparatını ve numuneyi kullanarak K_{IIC} değerleri ve mod II yorulma çatlak ilerleme hızları tespit edilmiştir.

Mod II kırılma tokluğu testi numuneleri ile mod II yorulma çatlağı ilerleme testi numunelerinin kırılma yüzeyleri, mod II yüklemenin etkilerini gözlemleyebilmek için fraktografik analize tabi tutulmuştur.

Bu alaşım için K_{IIC} değerleri, K_{IC} değerlerinin 1.3 ile 1.5 katı arasında ölçülmüştür. TL oryantasyonu, mod II yorulma çatlak ilerlemesine karşı en yüksek direnci göstermiştir.

Anahtar kelimeler: AA7050, mod II yorulma çatlağı ilerleme hızı, mod II kırılma tokluğu, kesme yüklemesi, mod II yüklemesi.

If not now, when?

ACKNOWLEDGEMENTS

I would like to express a great deal of thanks to my thesis supervisor Prof.Dr.Rıza Gürbüz for his valuable guidance and his advices in this study.

I am grateful to Ali Motameni Tabatabaei for his endless efforts and help in this study. He was with me when doing tests day and night.

I must also express my special thanks to my husband Emre Yurtoğlu, who helped, encouraged and made things easier for me in this study.

I want to thank Serkan Yılmaz for helping me in the SEM and also for his friendship.

I am grateful to all members of Metallurgical and Materials Engineering Department.

I am also grateful to Şevket Özdeş for his valuable help and answering me with patience.

I also want to thank my mother for her encouragement. She waited me in the mechanical laboratory till the sun rises when doing tests.

Finally, I want to thank Çisem Utku, Pınar Çömez and Çağlar Kök for their valuable friendship and endless encouragement in this study.

TABLE OF CONTENTS

LIST OF TABLES

TABLES

LIST OF FIGURES

FIGURES

CHAPTER 1

INTRODUCTION

Aluminum alloys are of great importance in aircraft industry for their high strength, toughness, low fatigue crack growth rate and resistance to corrosion. One of the favorable systems in aluminum alloys is 7XXX series.

7XXX series are heat treatable and preferred mostly for their high strength property. They are widely used in wing structures, bulkheads, longerons, stringers, etc. These structural parts of aircraft is subjected to primarily shear type of loading which means shear characteristics of these alloys have to be taken into account as well as their tensile characteristics.

Among the 7XXX alloys, 7050-T7451 alloy especially is used in aircraft systems due to its improved strength characteristics and stress corrosion cracking resistant characteristics. As it is important to know the shear characteristics, in this study, mode II fracture toughness values and mode II fatigue crack growth behavior of this alloy were investigated. A new loading frame and new type of specimens, which were used in a study of Banks-Sills and Arcan[1], were manufactured. By the help of this loading frame, these compact shear specimens were tested to reveal these characteristics. Also, due to heat-treated and rolled nature of this plate, the material is highly anisotropic and the tests were performed for two orientations which were designated as TL and LT directions.

CHAPTER 2

THEORY

2.1 Fatigue

In the middle of the nineteenth century failures were observed in bridges and railway components that were subjected to repeated loading. Because the loading was such that statically it would pose no problem, it was accepted very soon that the failures were a consequence of the cyclic nature of the loading. A complicating factor was that most failures occurred without any obvious warning. The problem was defined as metal fatigue, which was considered as a fracture phenomenon caused by repeated or cyclic loading [2].

A descriptive definition of fatigue is found in the report entitled General Principles for Fatigue Testing of Metals which was published in 1964 by the International Organization for Standardization in Geneva. In this report, fatigue is defined as a term which applies to changes in properties which can occur in a metallic material due to the repeated application of stresses or strains, although usually this term applies specially to those changes which lead to cracking or failure [3].

2.2 Fatigue Crack Growth

The fatigue fracture process can be separated into three stages: crack initiation, crack propagation, and final fracture.

Firstly, a fatigue crack is initiated at the specimen surface. The planes under high shear stress at the surface give rise to crack initiation at stage I. In this stage, crack growth rate is on the order of Angstroms per cycle. After the initial crack extends a few grains in length, stage II takes place and the crack propagates slowly across the specimen. The crack growth rate is relatively higher in stage II, which is on the order of microns per cycle. Lastly a static failure occurs on the last load cycle, when the net cross section has been adequately reduced.

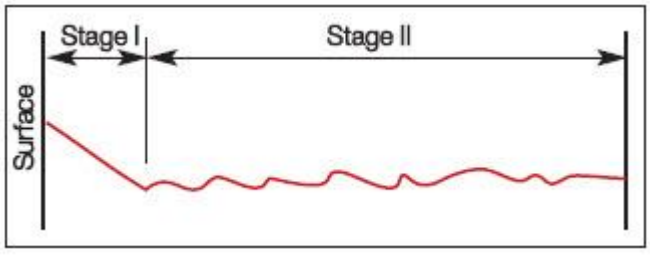

Figure 2. 1 Stage I and II of fatigue crack propagation [4].

Fatigue cracks are generally initiated at a free surface and at sites of high stress concentration such as a sharp corner or notch. There are also some cases where a fatigue crack starts in the interior of a carburized surface layer or nucleate at internal inhomogenities like inclusions.

Stage I, representing initiation stage, usually extends over only a small percentage of the fracture surface but may require many loading cycles if the nucleation process is slow. Often, stage I cracks assume an angle of about 45° in the xy plane with respect to the loading direction [5]. The nucleation of a fatigue crack for undamaged materials is proposed to take place with the formation of slip band extrusions and slip band intrusions [6]. Figure 2.2 illustrates schematically the concept of micro-deformation leading to the formation of a fatigue crack. Deformation would produce a contour at the metal surface as illustrated in Figure 2.2.a. In contrast, the back-and-forth fine slip movements of fatigue could build up notches (Fig.2.2.b) or ridges (Fig.2.2.c) at the surface. This would obviously be a stress raiser with a notch root of atomic dimensions. This situation can be the initiation of a fatigue crack. This mechanism shows that fatigue cracks begin at surfaces cracks have been found to initiate at slip-band intrusions [7].

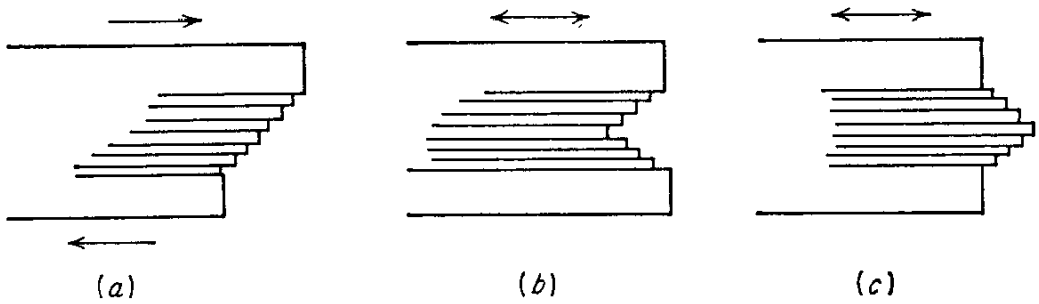

Figure 2. 2 Wood's model for crack initiation [6].

After a relatively short distance, the orientation of a stage I crack shifts to permit the crack to propagate in a direction normal to the loading direction. This transition has been associated with a changeover from single to multiple slip. The plane on which the stage II crack propagates depends on the relative stress state; that is, the extent of plane-strain or plane-stress conditions [5]. The scanning electron microscopy (SEM) of the fracture surface of stage II crack growth period shows an important feature of fatigue, namely the fatigue striations. Each striation represents the successive position of an advancing crack front that is normal to the greatest tensile stress. Each striation was produced by a single cycle of stress [7]. Therefore, it is possible to estimate the local fatigue crack growth rate in stage II simply by measuring the difference between two fatigue striations.

Stage II fatigue crack growth is occurred by a plastic blunting process [8] which is shown in Figure 2.3. Crack tip is sharp at the beginning of the loading cycle. When applied the tensile load, small double notch at the crack tip concentrates the slip along planes at 45° to the plane of the crack. Then the crack broadens to its maximum extension and it grows longer by plastic shearing and simultaneously tip becomes blunter. When the load is changed to compression the slip direction in the end zone is reversed. The crack faces are crushed together and the new crack surface created in tension is forced into the plane of crack where it partially folds by buckling to form a resharpened crack tip. Then resharpened crack will be blunted again in the next stress cycle [7].

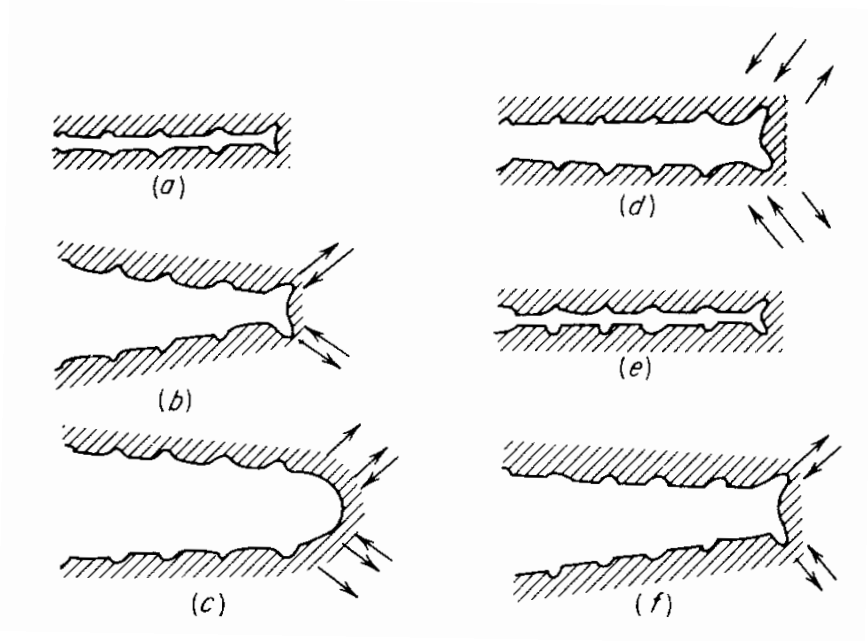

Figure 2. 3 Fatigue striation formation by plastic blunting process [8].

2.3 Fatigue Crack Growth Rate

Even though measures may be taken to minimize the possibility of fatigue failure, cracks and crack nucleation sites will always exist in structural components. Under the influence of cyclic stresses, cracks will inevitably form and grow; this process, if unabated, can ultimately lead to failure [9]. Results of fatigue studies have shown that the life of a structural component may be related to the rate of crack growth. Cracks can propagate from a barely detectable size to some critical length during stage II growth. Experimental techniques are available which are employed to monitor crack length during the cyclic stressing [9].

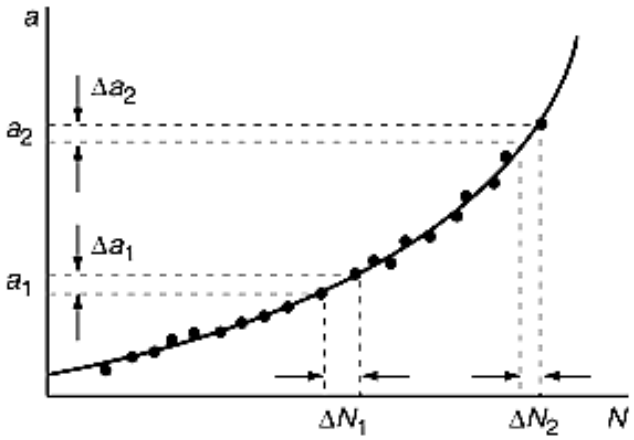

Figure 2. 4 Schematic fatigue crack growth curve, crack length (a) vs number of cycle (N) [10].

The fatigue crack growth rate, da/dN, is simply the slope of the a versus N curve (Fig.2.4) at a given crack length or given number of cycles, as identified by da/dN (Δa/ΔN).

When a material containing a crack is subjected to cyclic loading, the crack length (a) increases with the number of fatigue cycles, N, if the load amplitude (ΔP), load ratio (R), and cyclic frequency (v), are held constant. The crack growth rate, da/dN, increases as the crack length increases during a given test. The da/dN is also higher at any given crack length for tests performed at higher load amplitudes. Thus, the functional relationship below can be extracted from these observations:

$$\left(\frac{\mathrm{da}}{\mathrm{dN}}\right)_{\mathrm{R,v}} = \mathrm{f}(\Delta \mathrm{P}, \mathrm{a})$$

where the function f is dependent on the geometry of the specimen, the crack length, the loading configuration, and the cyclic loading range. This general relation is simplified by the use of the stress intensity range parameter, ΔK. The magnitude of the load range (ΔP) as well as the crack length and the geometry is defined by ΔK as follows:

$$\Delta \mathrm{K} = \mathrm{K}_{\mathrm{max}} - \mathrm{K}_{\mathrm{min}}$$

$$\mathrm{K}_{\mathrm{max}} = \mathrm{f}(\sigma_{\mathrm{max}}, \mathrm{a})$$

$$\mathrm{K}_{\mathrm{min}} = \mathrm{f}(\sigma_{\mathrm{min}}, \mathrm{a})$$

Stress intensity range can also be expressed in terms of stress ratio by the following relationships:

$$\Delta \mathrm{K} = (1 - \mathrm{R})\mathrm{K}_{\mathrm{max}} \text{ for } \mathrm{R} \geq 0$$

$$\Delta \mathrm{K} = \mathrm{K}_{\mathrm{max}} \text{ for } \mathrm{R} \leq 0$$

Results of fatigue crack growth rate tests for almost all metallic structural materials have shown that the da/dN versus ΔK curves have three distinguished regions [10]. A characteristic sigmoidal shape of this curve is shown in Figure 2.5. Region I shows a fatigue crack propagation threshold, ΔK_{th}, which corresponds to the stress-intensity factor range below which cracks do not propagate. With increasing ΔK, the crack growth rate increases rapidly above this value. Region II, which is also called Paris region, shows essentially a linear relationship between log da/dN and log ΔK. In region III, the fatigue crack growth rates are very high as they come close to instability, and little fatigue crack growth life is left. In this region, accelerated fatigue crack growth is observed and K_{max} approaches K_c, fracture toughness of the material.

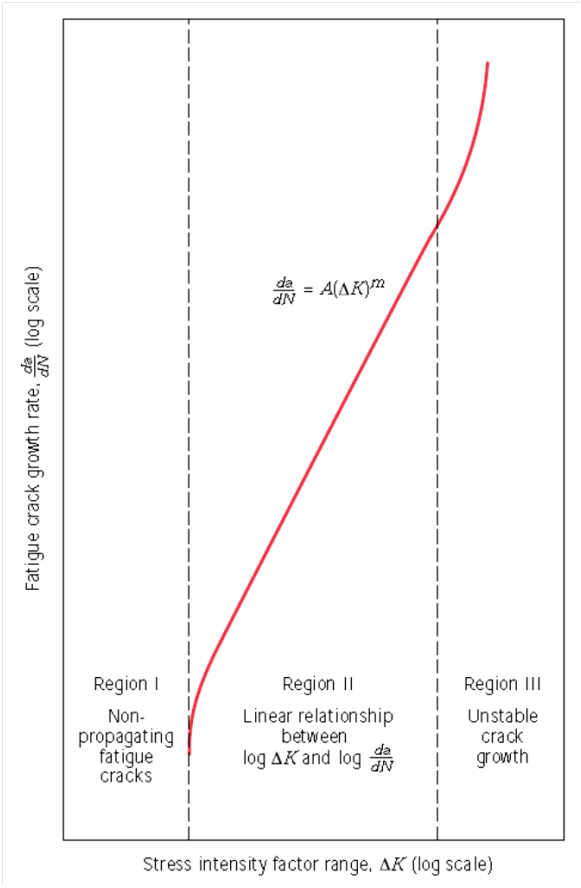

Figure 2. 5 Schematic representation of logarithm fatigue crack growth rate da/dN vs logarithm stress intensity factor range ΔK [10].

There are many studies describing the crack growth rate curve in semi- or wholly empirical manner. The first and most widely applied model is published by Paris and Erdoğan in 1963 [11]:

$$\frac{\mathrm{da}}{\mathrm{dN}} = \mathrm{C}(\Delta\mathrm{K})^{\mathrm{m}}$$

where C and m are constants of material and they are obtained from the intercept from the plot shown in Figure 2.5. The constant C is proposed to include the effects of the material, mean load, loading frequencies and environment. The constant m is an empirical constant which is in the range of 2 and 7. The exponent m is between 2 and 4 for ductile materials [3].

Paris equation is applicable for a single mode of farfield loading. For tensile fatigue, it is understood that ΔK refers to the range of mode I stress intensity factors during the stress cycle. Likely, a stress intensity factor range ΔKII or ΔKIII can also be used in Paris equation to characterize fatigue crack growth in mode II or mode III, respectively [3]. Fatigue life of a material can be estimated by knowing the fracture toughness and the empirical constants in the Paris-Erdoğan equation.

In 1967, Forman et al. [12] developed an equation to specify crack growth rate for both stage II and III:

$$\frac{da}{dN} = \frac{C(\Delta K)^m}{(1-R)(K_c - \Delta K)}$$

where K_c is the critical stress intensity factor. It shows the growth rate to depend upon R and should therefore apply for all R values: the equation pretends to know how da/dN depends on R [13].

In 1972, Pearson et al. [14], modified the equation for fatigue crack growth below the threshold level:

$$\frac{da}{dN} = \frac{C(\Delta K)^m}{[(1-R)(K_c - \Delta K)]^{1/2}}$$

Ewalds and Wanhill [15] then proposed a formula to describe the whole sigmoidal curve by the following formula:

$$\frac{da}{dN} = C\Delta K^m \left[\frac{1-\left(\frac{\Delta K_{th}}{\Delta K}\right)^{n_1}}{1-\left(\frac{\Delta K_{max}}{\Delta K}\right)^{n_2}}\right]^{n_3}$$

where ΔK_{th} is the near threshold intensity factor and n_1, n_2 and n_3 are empirically determined constants.

2.4 Mode II Fatigue Crack Growth

There are three modes of loading affecting on a material (Fig.2.6). These are tensile, shear and tear type of loading modes and also they are known as mode I, mode II and mode III type of loadings, respectively.

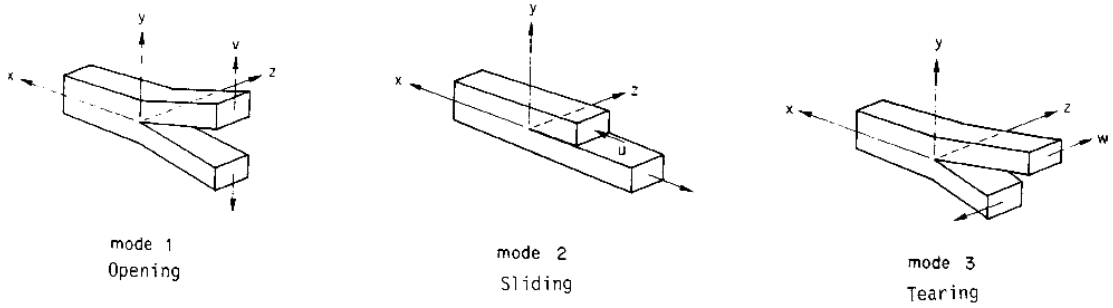

Figure 2. 6 Crack Opening Modes: (a) Mode I – Opening Mode, (b) Mode II – Shearing Mode, (c) Mode III – Tearing Mode [16].

A.A.Merati et al. [17] explained that many structural parts of aircraft is primarily subjected to shear type of loading such as fuselage lap joints and fasteners used on skin, spar and web joints of wings. For this reason, mode II fatigue crack growth is of great importance for aircraft and also for many other systems.

Since there is no standard for revealing mode II fatigue crack growth property for a material, many researches have been made to determine this property. Studies under mode II loading conditions were held to determine K_{IIC} values [1,18-21] and mode II fatigue crack growth behavior [22-27] of the materials.

D.L.Jones and D.B.Chisholm [18] in their study, developed a new specimen and tested 2024-T4 aluminum alloy for its mode II fracture toughness value. They obtained an average value of 43.4 MPa$\sqrt{m}$, which is 1.15 times the K_{IC} value of this alloy. W.Hiese and J.F.Kalthoff [19] with their modified loading fixture also determined that K_{IIC} value of the aluminum alloy 7075 is 1.5 times the corresponding K_{IC} value. N.Tsangarakis [21] studied two different aluminum alloys which are 5083-H131 and 2519-T87 and determined their all modes fracture toughness values experimentally. The results show that K_{IIC} values of the alloys are at about maximum 1.35 times of their K_{IC} values.

L.Banks-Sills and M.Arcan [1], also developed a new specimen and a method to determine mode II fracture toughness of the materials. Perspex material is used for the test. Derived formulas shed light on further studies concerning mode II fracture toughness and also mode II fatigue crack growth behaviors of the materials.

R.J.Buzzard et al.[22] developed a specimen and a method to understand the mode II fatigue crack growth. Specimens were made of 7075-T6 aluminum alloy. Test frequency was 2 Hz at a maximum load of 13789 N and the stress ratio (R) was 0.1. In this study, a vs. N graph was plotted (Fig.2.7). The test was held up to 5000 cycle and the corresponding crack length is about 11 mm.

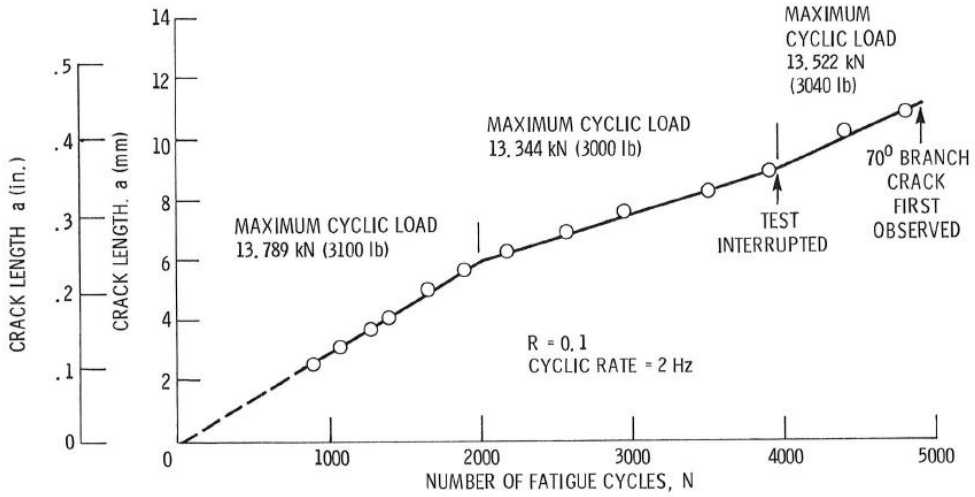

Figure 2. 7 Crack length vs number of cycles graph [22].

In another study [23], Murakami and Hamada improved a new method and measured the mode II crack growth rate for a low strength carbon structural steel and a rail steel. However, the main aim was to measure the mode II threshold stress intensity range, ΔK_{th}.

Otsuka et al. [24] also developed a new device to determine the fatigue crack growth characteristics of hard materials under mode II loading. They used a high carbon chromium bearing steel and a 0.75% carbon steel and obtained da/dN vs. ΔK_{II} relationships for these materials.

Wang et al.[25], Otsuka et al.[26], and K.Makoto et al.[27] also investigated the behavior of fatigue crack growth for many materials including specific aluminum alloys such as 2024-T3 and 7075-T6 and obtained relationships between da/dN and ΔK_{II}.

2.5 Effect of Material Orientation on Crack Growth

Since the crack propagation is local, it is affected by metallurgical features such as microstructure and inclusions.

Most metallic materials used in manufacturing and construction have undergone melting and casting, and subsequent metal-working processes, such as forging and rolling. They contain precipitates that are formed from the addition of alloying elements that can improve their machinability. These particles tend to segregate to grain boundaries, and tend to degrade the material's fracture resistance in relation to its grain size and orientation. As such, their fracture toughness, along with their strengths, depends on their orientation. These orientations of sheet and plate products are typically defined in relation to their primary rolling direction, which is designated as the longitudinal (L) direction. The width direction is designated as the transverse (T), or long-transverse direction. The thickness direction is also transverse to the rolling direction, but is designated as the "short-transverse" (S) direction.

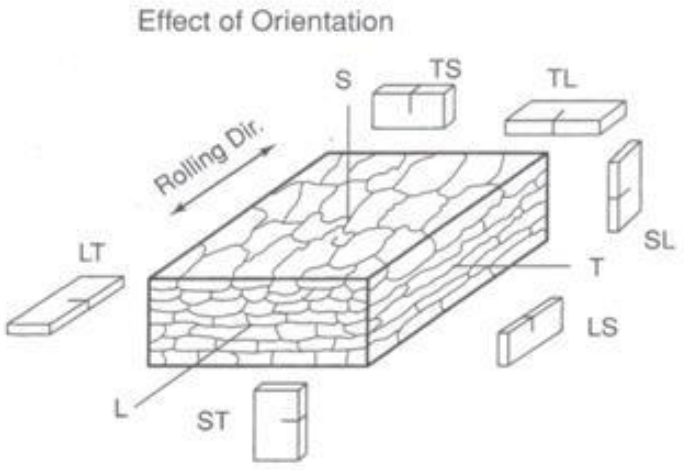

Figure 2. 8 Schematic illustration of grain structure in a rolled plate, along with designations and the associated cracking planes and crack growth directions [28].

Orientation dependence is principally a result of heterogeneities introduced by the processes used in its creation. During rolling, for example, inclusion particles tend to be broken and distributed along boundaries that become parallel to the rolling, or the S plane. As such, the lowest fracture toughness tends to be associated with the short-transverse (SL and ST) orientations [28].

2.6 Al-Zn-Mg-Cu Alloys (7XXX Alloys)

The 7XXX alloys are heat treatable and, among the Al-Zn-Mg-Cu versions in particular, provide the highest strengths of all aluminum alloys. As the aircraft industry requires fracture-critical designs, this requirement provided the driving force to develop high-toughness alloy; therefore the widest application of the 7XXX alloys has been aircraft industry.There are several alloys in the series that are produced especially for their high toughness, notably 7050, 7150, 7175, and 7475; for these alloys, controlled impurity levels, particularly of Fe and Si, maximize the combination of strength and fracture toughness. Forgings of these alloys are commonly used for large structural members in aircraft [12].

The 7XXX alloys are commonly used in primary and secondary structures of aircraft such as wing structures, longerons, bulkheads, frames, stringers and skins, etc [17].

Among the 7XXX alloys, 7050-T7451 aluminum alloy is used in aircraft systems both in military and commercial applications to a great extent because of its improved stress corrosion cracking resistance and strength characteristics. Rolling and heat treating makes this material highly anisotropic. [29].

2.6.1 Composition

The amount of Zn is generally higher than Mg. The best strength and response to heat treatment is obtained by high Zn/Mg ratios. The ratios over 2 result in the formation of $MgZn_2$ while at lower ratios, $Mg_3Zn_3Al_2$ forms. The best fatigue resistance is also obtained at lower Zn/Mg ratios [30].

Precipitation order in Al-Zn-Mg-Cu alloys can take many forms depending on heat treatment conditions such as quenching and aging. The phases formed depend on aging temperature higher than the position of the alloy in the phase diagram [31]. Possible intermetallic phases which can occur below the solidus are reported in some studies [32-34] and they are $\eta(MgZn_2)$, $T(Al_2Mg_3Zn_3)$, $S(Al_2CuMg)$, $\theta(Al_2Cu)$ Al_7Cu_2Fe, $Al_{13}Fe_4$ and Mg_2Si. Second-phase particles are known to influence fatigue behavior in high-strength aluminum alloys [35].

2.6.2 Heat Treatment of the Al-Zn-Mg-Cu System

Among all aluminum alloys, Al-Zn-Mg-Cu system have the highest response to age hardening [31]. The heat treatments that are normally used for 7XXX series alloys are designed to produce a very high density of fine GP zones or precipitates that strongly interact with dislocations and thereby increase the yield strength of the alloy. A typical heat treatment program for these alloy systems consists of an initial solution heat treatment, which dissolves particular alloying elements. This is followed by quenching, which is designed to retain a high level of the dissolved elements in supersaturated solid solution. In this condition, the alloy can be given an aging heat treatment to achieve the required temper [36].

In the 7XXX series the reaction sequence, which occurs with increasing time, is:

$$\text{Supersaturated Solid Solution} \rightarrow \text{Guinier} - \text{Preston Zones} \rightarrow \eta^1 \rightarrow \eta(MgZn_2) \rightarrow T[(AlZn)_{49}Mg_{32}]$$

Maximum hardness is obtained when the matrix contains semi-coherent η^1phase. When the aging time is less than the peak aged condition, it is called as underaged and as the opposite when the aging time is higher than the peak aged condition, it is called as overaged.

In 7XXX series aluminum alloys, the boundary most likely contains η phase ($MgZn_2$) and T phase [$(AlZn)_{49}Mg_{32}$] depending on the aging time [37].

In many cases, unless the sample is rapidly quenched into water, the precipitates may actually nucleate during the solution heat treatment. They will initially be very fine and closely spaced. As aging proceeds, they will coarsen and their spacing will increase [37].

A depletion of Mg and Zn occurs around the η and T phases. As the aging time increases, these zones usually become more and more depleted. These solute depleted zones are called Precipitate Free Zones (PFZ) [37].

After solution heat treatment and quenching, precipitation heat treatment following applied to 7XXX series aluminum alloys are designated as T6 and T7 tempers. T6 means solution treated and then artificially aged aluminum alloy and T7 means solution heat treated and then overaged, which means that some degree of strength has been sacrificed to improve one or more other characteristics such as to obtain higher strength. Special treatment, which is T74 temper, is applied by the suppliers to increase the combination of strength, toughness and corrosion resistance. And T7XX51 temper is applied for stress relieving by stretching.

Alloys in T6 tempers generally have the highest strengths. Alloys in T7 tempers have lower strength than that of T6 tempers but that means some degree of the strength has been sacrificed to improve dimensional stability or to lower residual stresses.

The T73 tempers is a group of T7 tempers and this heat treatment procedure is conducted as either two-stage isothermal precipitation or as heating at a controlled rate to a single treatment temperature. The purpose is to produce GP zones that will not dissolve but transform to the η^1precipitate when heated to the aging temperature above 150°C. Thus, either time or the temperature of the first step or the rate of heating must be controlled to achieve this [38].

CHAPTER 3

EXPERIMENTAL PROCEDURE

3.1 Material

The material used in this study was a cold rolled plate of AA7050 T7451 aluminum alloy. The thickness of the plate was 35 mm and there is no variation in the hardness profile (avg. 167HV5) through the thickness. The chemical composition in the standard and the actual composition of the alloy AA7050, in weight percentages are shown in the Table 3.1.

Table 3. 1 The chemical composition of AA7050 alloy in weight percentages.

	Al	**Zn**	**Mg**	**Cu**	**Zr**	**Ti**	**Cr**	**Si**	**Fe**	**Mn**
Min.	87.3	5.7	1.9	2.0	0.08	-	-	-	-	-
Max.	90.3	6.7	2.6	2.6	0.15	0.06	0.04	0.12	0.15	0.10
Actual	88.5	6.22	2.40	2.43	0.158	0.0519	0.063	0.0320	0.0803	<0.0010

Heat treatment type of the material is T7451. This kind of heat treatment requires a solution heat treatment at 477°C, followed by double aging at 121°C for 24 hours and at 163°C for 24 hours. Heat treatment was applied to this plate by the supplier, ALCOA. The microstructure of the plate is shown in Figure 3.1.

Through the thickness, microstructure was examined and the structure was homogeneous in every point. Fine intermetallic compounds (Al_7Cu_2Fe, Mg_2Si, and Al_2CuMg) were observed throughout the structure and larger intermetallic compounds were found among the recrystallized grains. Recrystallized grains flattened in the short transverse (S) direction and elongated grains observed especially in longitudinal (L) direction are of cold rolling process. Also, one third of the microstructure is recrystallized due to its close aging temperatures to its recrystallization temperature. Aspect ratio is 1 for recrystallized grains, and the ratio goes up to 5 for elongated grains.

Average grain size of the material is about 13 μm. For the elongated grains through the short transverse direction, average grain size is nearly 21 μm and for the same grains through the longitudinal direction, average grain size is nearly 110 μm.

Differences in the microstructures for different directions lead to variations in mechanical properties. Tensile properties, hardness values, impact toughness values were determined and all of the tests for characterizing the material were performed in the laboratories of the Metallurgical and Materials Engineering Department.

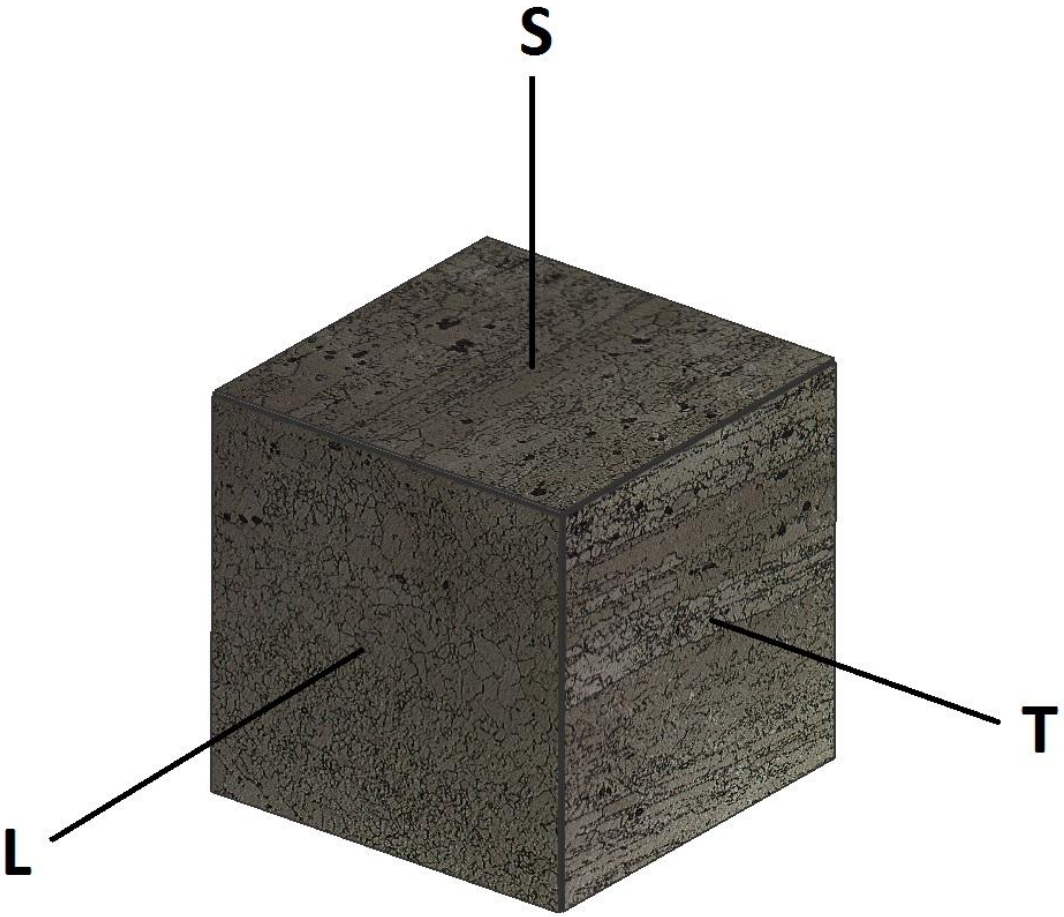

Figure 3. 1 The microstructures in 3 directions, (200X).

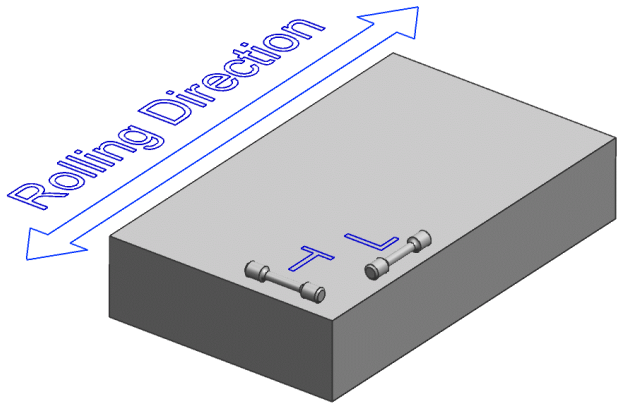

Figure 3. 2 Directions of tensile specimens in the plate.

Tensile tests were carried out according to the related standard [39] for tensile testing of metallic materials on the Instron testing machine with a capacity of 10 tons. Specimens taken out from the plate in two directions as shown in the Figure 3.2. Gage lengths of the specimens were 40.25 mm.

Hardness measurements were conducted on the EMCO Test testing machine which applies a 5 kg preload. The test standard for this test is ASTM E384 - 11e1 [40]. Measurements are from three surfaces of the plate.

Determination of impact toughness values was done on the Tinius Olsen testing machine with an impact energy of 300 KV. The test standard for this test is ASTM E23-07ae1 [41]. Specimens removed from the plate as shown in the Figure 3.3.

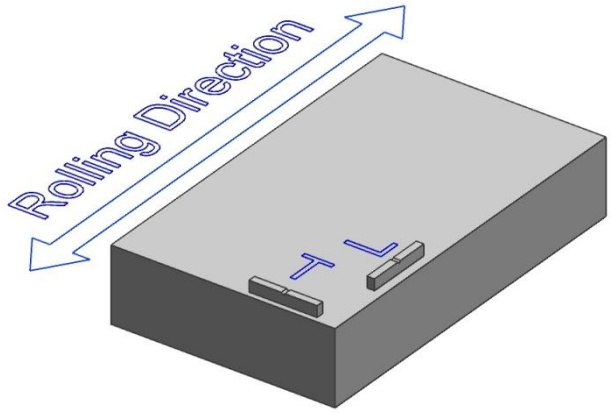

Figure 3. 3 Directions of impact toughness specimens.

Fracture toughness measurement was done on the MTS testing machine according to the related standard of ASTM [42]. Specimens (Fig.3.4) were taken out from the plate in two orientations which are TL and LT directions.

Figure 3. 4 Fracture toughness specimen.

3.2 Testing Specimen

In this study, specimens, called compact shear specimen, were prepared according to the study of Banks-Sills L. and Arcan M [1]. The specimen (Fig.3.5) was designed mainly to find out the K_{IIC} values of the materials by using the loading frame shown in Figure 3.6.

The shape of the compact shear specimen is designed to obtain the shear stress concentration at the region between DD and DD.

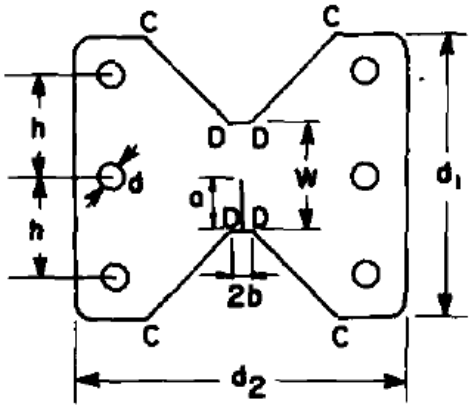

Figure 3. 5 The compact shear specimen with crack length a (W=30mm, 2b=6mm, d_1=82mm, d_2=98mm, d=8mm, h=31mm) [1].

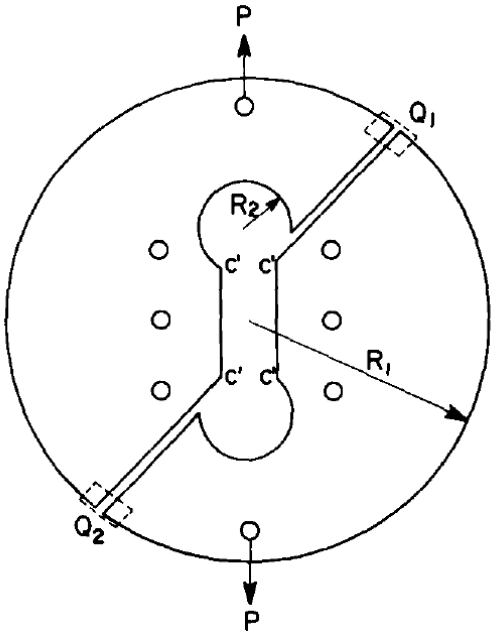

Figure 3. 6 Loading frame (R_1=95mm, R_2=20mm) [1].

The load is applied as shown in the Figure 3.6 so that pure shear region on the specimen can be created.

Straight-through notch starter configuration was used on the specimens which were described in ASTM E647 and ASTM E399.

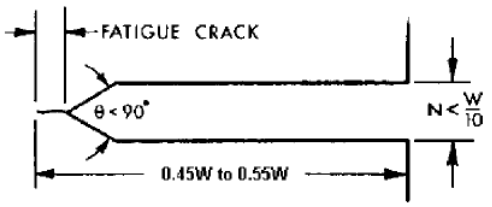

Figure 3. 7 Straight through notch style [42].

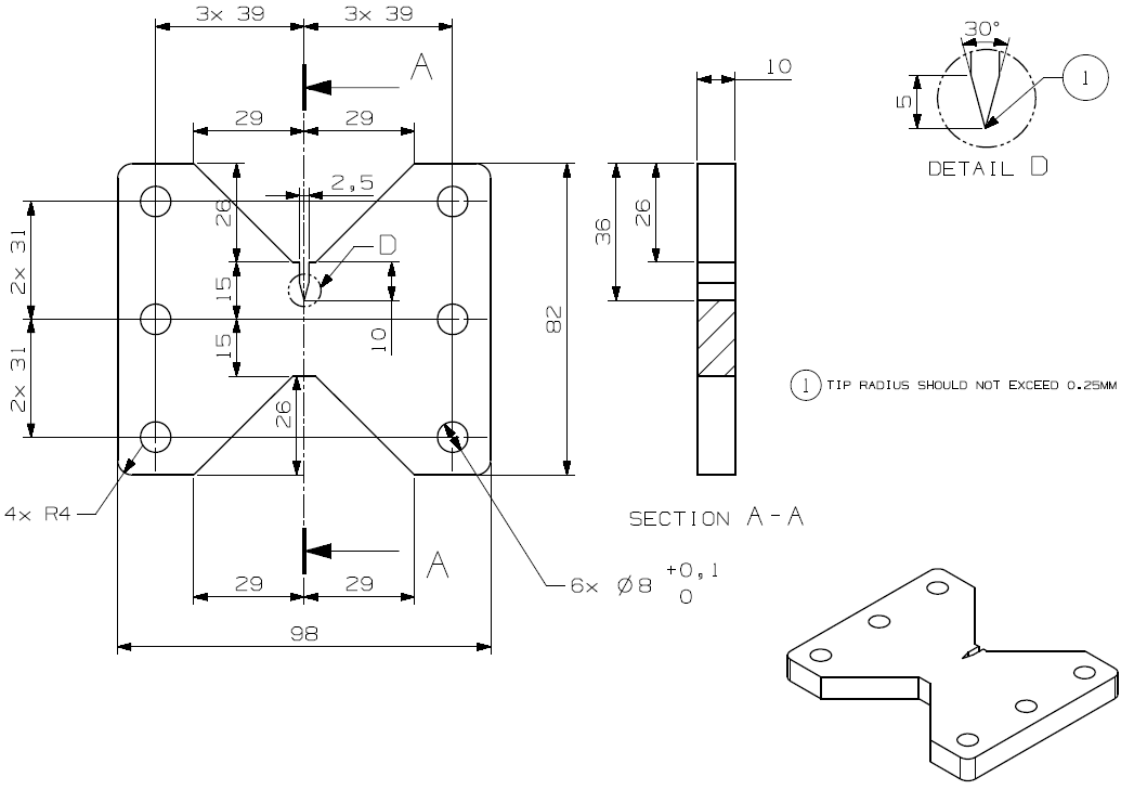

Figure 3. 8 Technical drawing of the compact shear specimen.

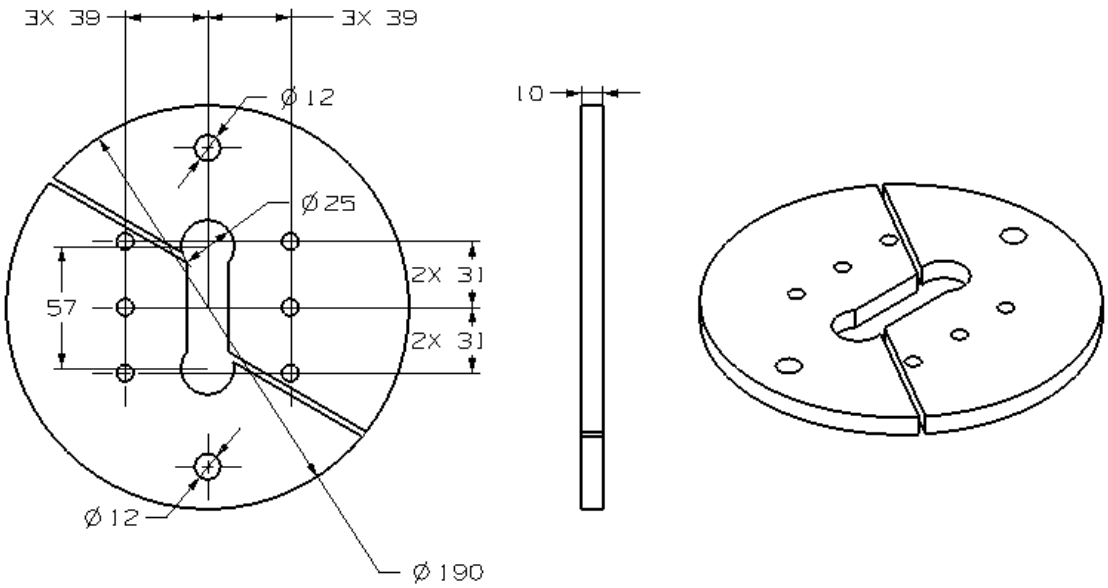

Figure 3. 9 Technical drawing of the loading frame.

Specimen (Fig.3.8) and the loading frame (Fig.3.9) were modeled at UniGraphics and manufactured in Ostim.

Specimens were machined by two processes. To take the specimens from the plate evenly and to have less remaining plate, wire EDM was used and CNC machining was used to give the last shape to specimens. Specimens in the same orientation were taken out from the same thickness as the plate is homogeneous. The final shape of the specimen after CNC machining is shown in Figure 3.10.

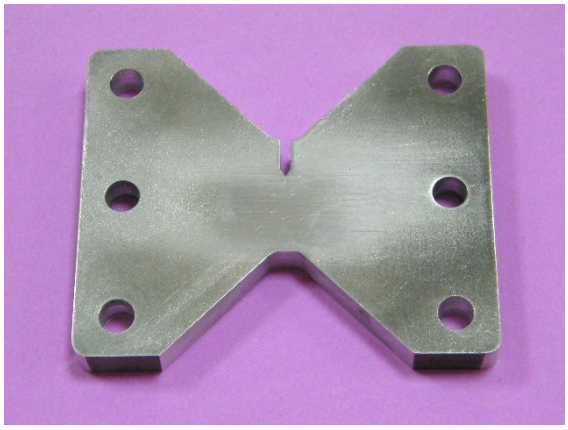

Figure 3. 10 The compact shear specimen.

The tests were carried on for two orientations which are TL and LT. Notations for orientations are shown in Figure 3.11. First letter indicates the direction normal to the crack plane and the second letter indicates the anticipated direction.

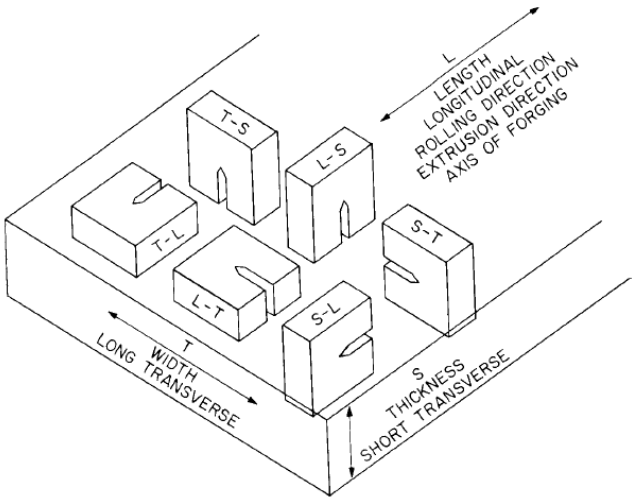

Figure 3. 11 Notations for the orientations [42].

3.3 Testing the Material

All tests were performed on a closed – loop, servo – controlled hydraulically activated MTS 810 testing machine which has a 10 tons capacity.

All the crack growth measurements for fracture toughness precracking and also for fatigue crack growth tests were done optically by using a travelling microscope with a resolution of ± 0.01 mm. As crack foils do not work in shear type of loading, they could not be used in this study. Also one travelling microscope was available; therefore, measurements were done from the front surface of the specimens because of technical limitations.

Fracture toughness data were taken from the data acquisition system provided by the movement of the head of the MTS testing machine.

K_{IIC} values and mode II fatigue crack growth behavior of AA7050 T7451 aluminum alloy will be obtained in two directions, TL and LT.

All the tests were performed at the room temperature.

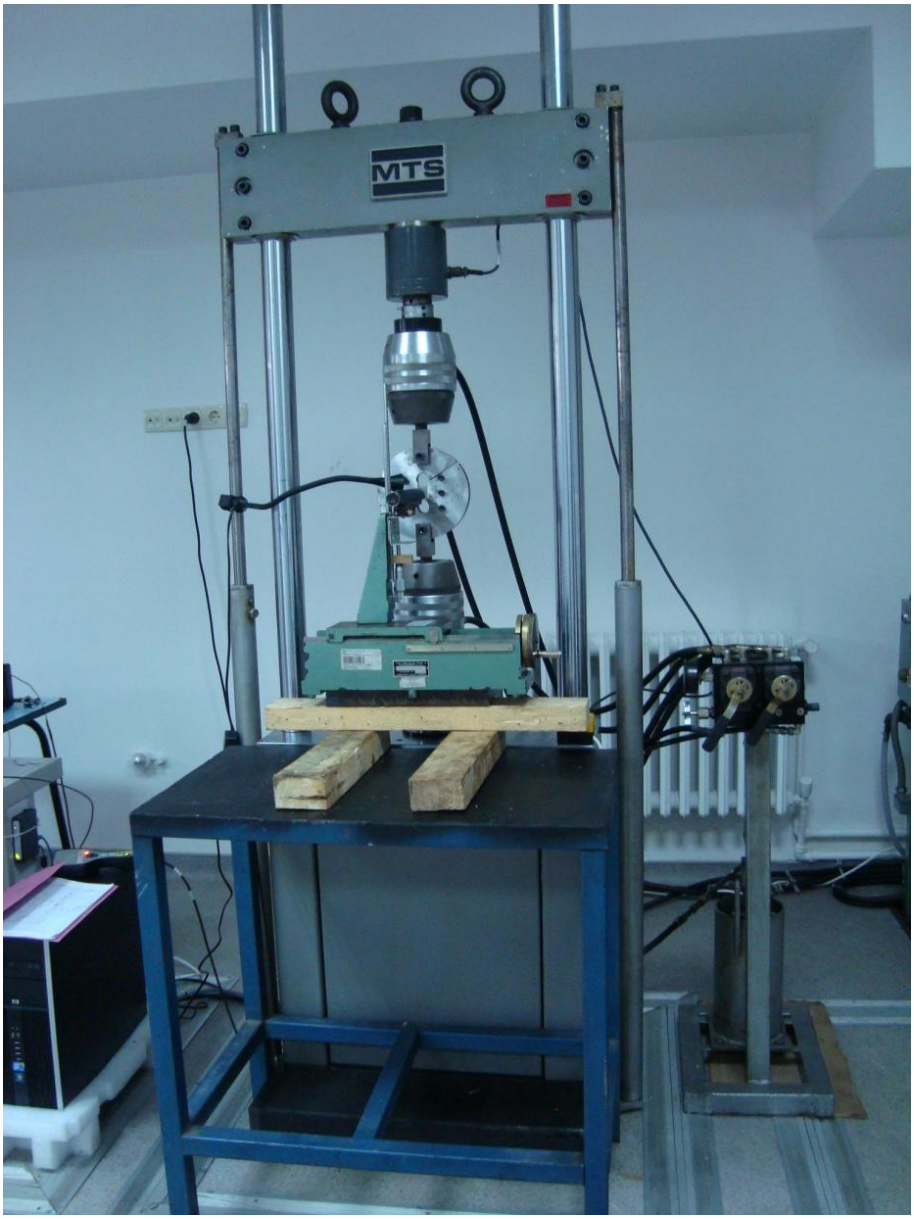

Figure 3. 12 MTS Testing Machine.

3.3.1 K_{IIC} Testing

To determine the critical force for growing the fatigue crack, K_{IIC} values of the AA7050 T7451 aluminum alloy in two directions are required. This study is based on Banks-Sills and Arcan's study [1] and the method for determining the K_{IIC} value is used.

Fatigue precracking configuration indicated in Figure 3.13 is used for aluminum and steel specimens. Precracking was done under mode I loading as Banks-Sills and Arcan in their study used this type of loading for precracking. Specimen fixed to the machine for fatigue precracking is shown in Figure 3.14.

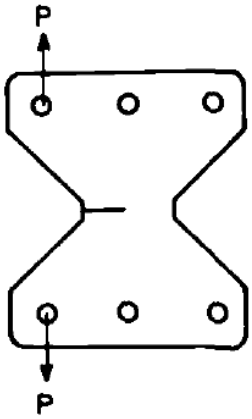

Figure 3. 13 Loading illustration of the compact shear specimen for fatigue precracking [1].

Figure 3. 14 Loading the specimen for fatigue precracking on MTS testing machine.

For this loading type, the formula below was used in determining the applied load required for fatigue precracking the compact shear specimen.

$$K_I = \frac{P\sqrt{\pi a}}{Wt}\left[5.528 - 42.29\left(\frac{a}{W}\right) + 159.8\left(\frac{a}{W}\right)^2 - 254.1\left(\frac{a}{W}\right)^3 + 162.5\left(\frac{a}{W}\right)^4\right]$$

where,
P : Maximum precrack load
a : Crack length
W : Specimen width
t : Specimen thickness

According to ASTM E399, the standard specified crack size ranges from 0.45W to 0.55W and was the total size of the starter notch slot plus fatigue crack. In this study, specimens were marked as the fatigue precracks will be approximately 0.45 times the width (Fig.3.15).

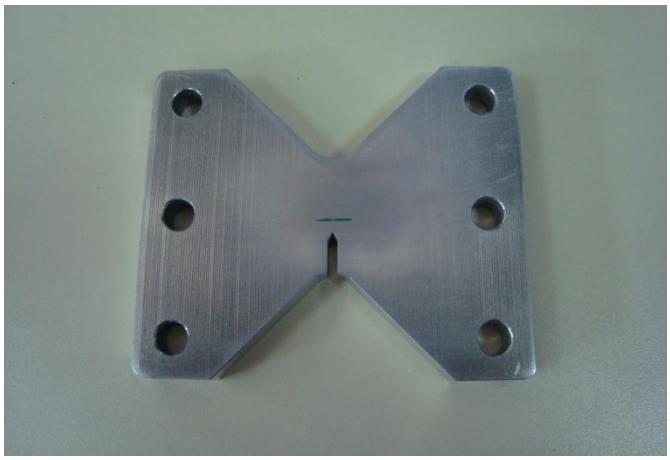

Figure 3. 15 Compact shear specimen with a mark indicating the fatigue precrack limit.

After the notch was extended with a fatigue crack, the specimen was inserted into the loading frame and loaded to fracture. Loading rate was 0.5 kN/sec. Then K_{IIC} was calculated by using the formula below and in the same way described in ASTM E399.

$$K_{II} = \frac{P\sqrt{\pi a}}{Wt}\left[1.006 - 0.313\left(\frac{a}{W}\right) + 3.344\left(\frac{a}{W}\right)^2 - 6.691\left(\frac{a}{W}\right)^3 + 5.649\left(\frac{a}{W}\right)^4\right]$$

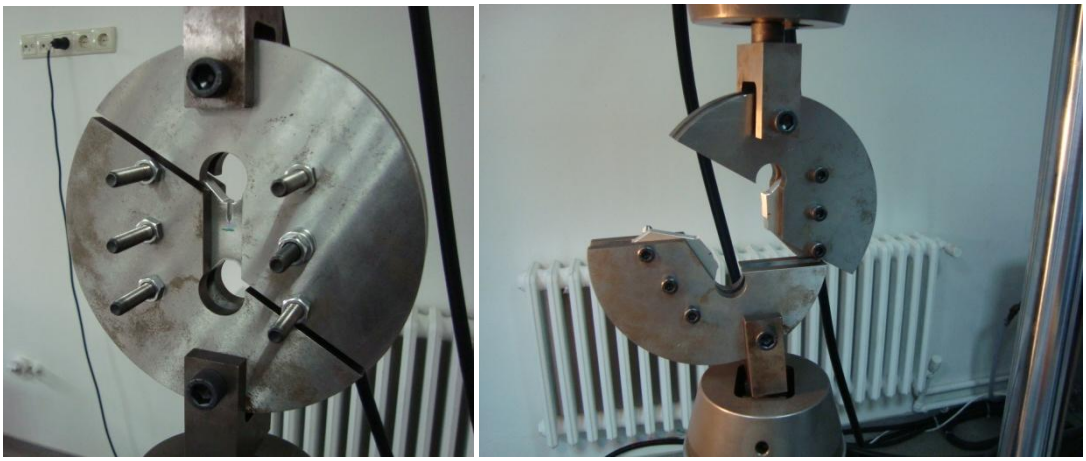

a **b**

Figure 3. 16 a) Specimen inserted in the loading frame. b) Specimen and the loading frame after fracture

3.3.2 Mode II Fatigue Crack Growth Testing

Fatigue crack growth tests under mode II loading were held on according to the study of Banks-Sills and Arcan [1].

All the compact shear specimens were precracked with the calculated load by the K_I formula. Stress ratio, R was 0.1 and frequency was 5 Hz. As in the K_{IIC} testing, lengths of the fatigue precracks were kept between 0.45W and 0.55W, which corresponds to 13.5 mm - 16.5 mm interval. Precracking process was held in the same way as in the K_{IIC} testing.

Fatigue crack growth tests were conducted by constant amplitude sinusoidal load waves with a frequency of 1 Hz and the stress ratio, R was -1 as the crack path deviated from its direction. Applied load for growing the fatigue crack was calculated by the K_{II} formula.

Specimens were marked in 0.5 mm intervals and growing of the fatigue cracks were observed by the travelling microscope with the help of the light attached to the MTS testing machine (Fig.3.17).

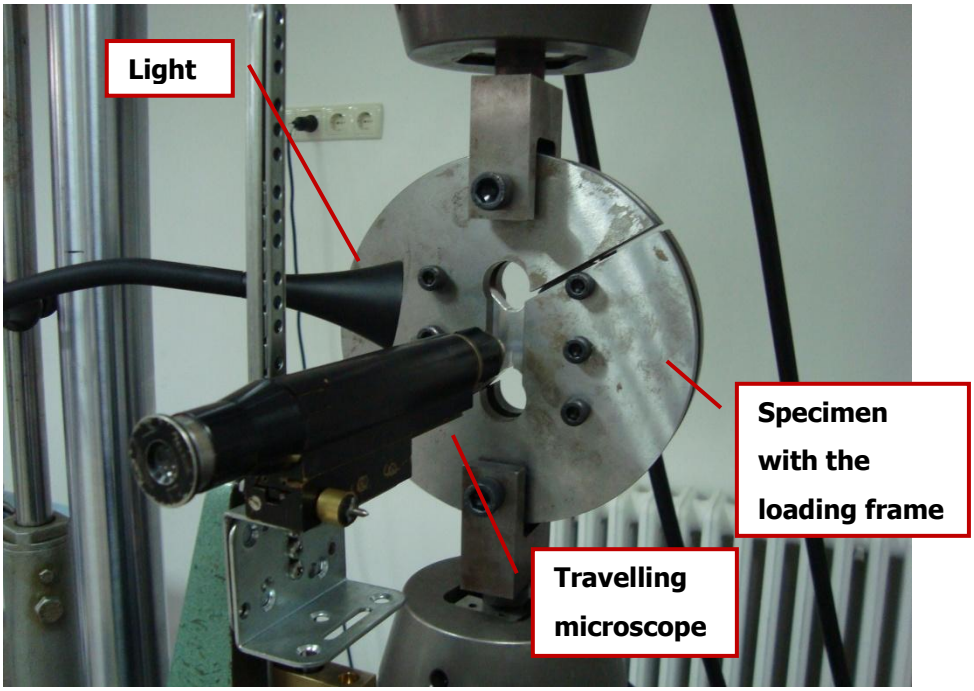

Figure 3.17 Fatigue crack growth test under mode II loading.

3.4 Fractography

Fracture surfaces of the specimens were macro-examined and photographed. Then, these surfaces were cut from the specimens for scanning electron microscope examinations. Micrographs were taken from the fracture surfaces.

3.5 Visualization of Shear Concentration on FEM Model

Finite element model of the specimen was done to visualize the stress flow and stress concentrations on the specimen. For this purpose, to make the FEM model PATRAN2005 was used and NASTRAN2005 was used as solver.

CHAPTER 4

RESULTS AND DISCUSSION

4.1 Mechanical Properties

A series of tests were applied to characterize the material's mechanical properties. First, tension tests were done according to the EN 10002-1 [39]. Engineering stress-strain curves are shown in Figure 4.1 and 4.2, and the values measured are given in the Table 4.1. Tensile strength in the rolling direction (L) is greater than that of normal to the rolling direction (T).

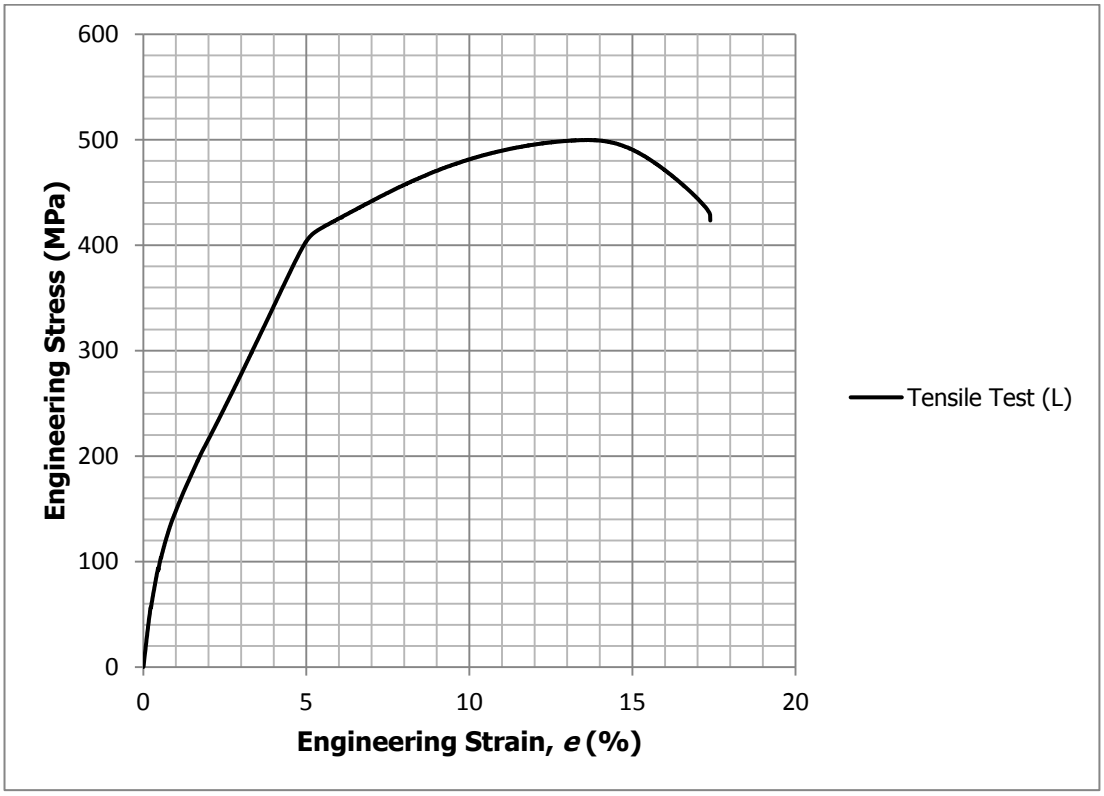

Figure 4. 1 Graph of the tensile test in L direction- in the rolling direction.

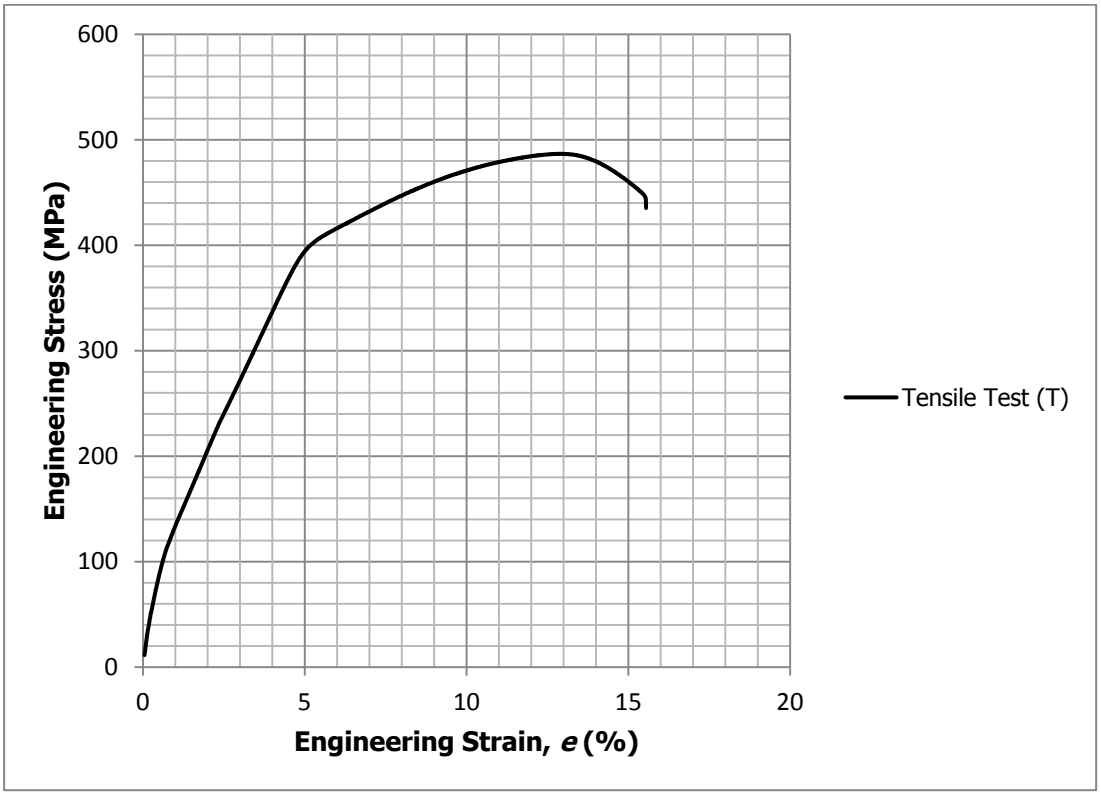

Figure 4. 2 Graph of the tensile test in T direction- normal to the rolling direction.

Table 4. 1 Tensile values of the test material in two directions.

Orientation	Tensile Strength (MPa)	Yield Strength (MPa)	% Elongation
L	498	410	13.75
T	486	390	12.75

Hardness values which were measured according to the ASTM E384 - 11e1 [40] are given in the Table 4.2.

Table 4. 2 Hardness values of the test material in three directions.

Orientation	Hardness (HV5)
S	166 ± 1
T	168 ± 1
L	168 ± 2

Also, impact toughness values for two directions were determined according to ASTM E23 - 07ae1 [41] and given in Table 4.3.

Table 4. 3 Impact toughness values of the test material at room temperature.

Orientation	Impact toughness (Joule) (Avg)
L	6.0 ± 1.2
T	4.7 ± 0.3

Fracture toughness values were determined according to the ASTM E399 – 09e2 [42]. Stress ratio (R) for precracking was 0.1 and frequency was set as 5 Hz. In Figure 4.3 and 4.4, load vs displacement graphs are shown. The red line represents the linear portion of the test record and the blue line is the 0.95 times the slope of the red line. K_{IC} values, which are given in Table 4.4, were calculated according to the value of the intersection point of the main test record curve and the blue line. The equation used for calculating the K_{IC} values is given below:

$$K_Q = \frac{P_Q}{\sqrt{BB_N}\sqrt{W}} . f\left(\frac{a}{W}\right)$$

$$f\left(\frac{a}{W}\right) = \frac{\left(2+\frac{a}{W}\right)\left[0.886 + 4.64\frac{a}{W} - 13.32\left(\frac{a}{W}\right)^2 + 14.72\left(\frac{a}{W}\right)^3 - 5.6\left(\frac{a}{W}\right)^4\right]}{\left(1-\frac{a}{W}\right)^{3/2}}$$

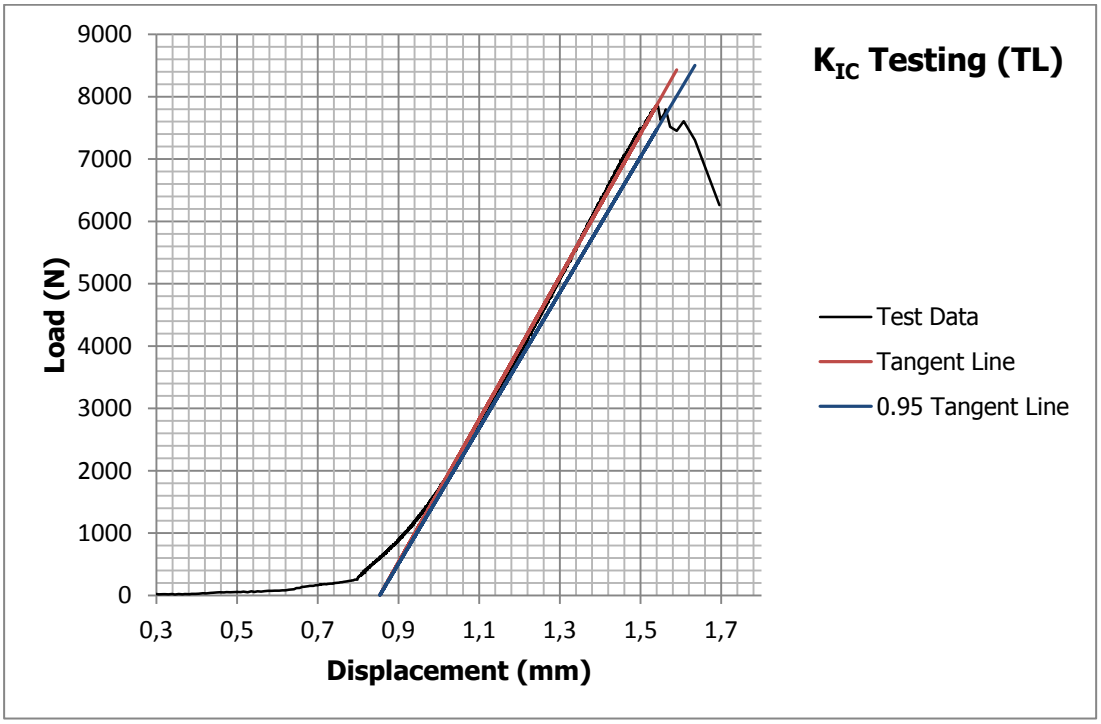

Figure 4. 3 Load vs displacement plot of fracture toughness test for TL direction.

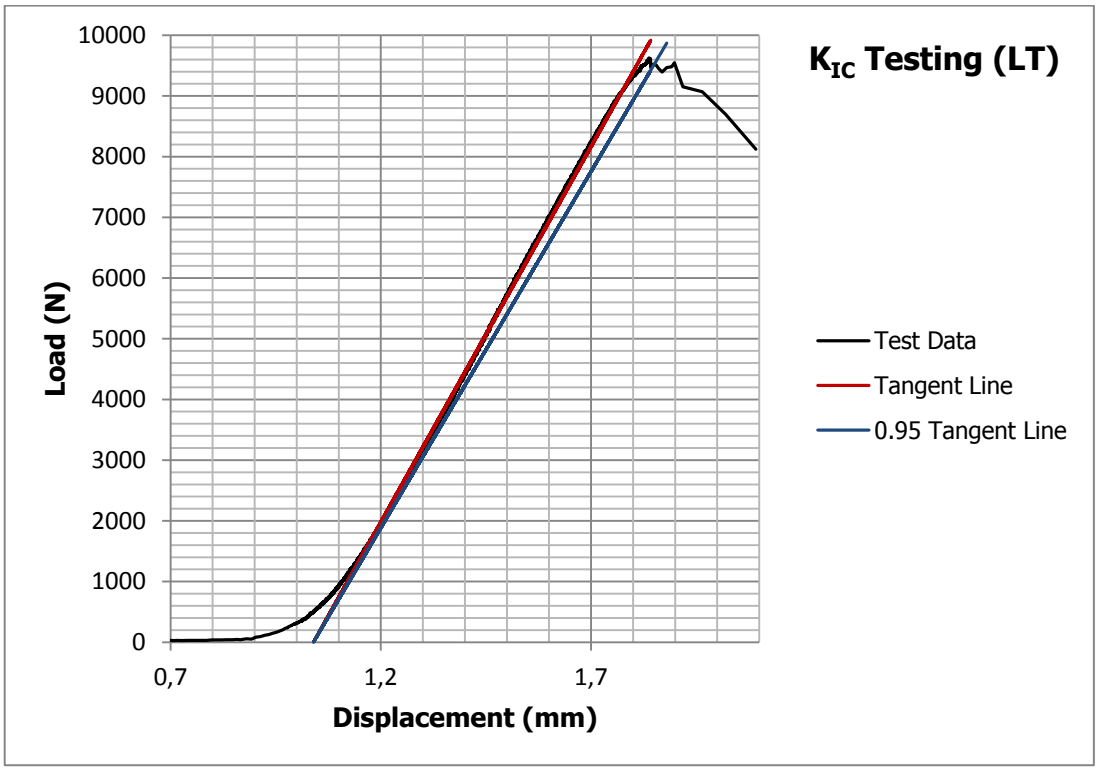

Figure 4. 4 Load vs displacement plot of fracture toughness test for LT direction.

Table 4. 4 Plain-strain fracture toughness values of the test material in two orientations.

Orientation	**K_{IC} (MPa$\sqrt{m}$)**
TL	26.1
LT	32.1

4.2 Mode II Fracture Toughness (K_{IIC}) Values

In order to determine the K_{IIC} values of the AA7050 T7451 aluminum alloy for TL and LT directions, 2 specimens were tested in each direction.

Calculated load for fatigue precrack was around 3000N and as the stress ratio (R) was 0.1, applied load was set between 300 N and 3000 N. The frequency of loading was 5 Hz.

After precracking, specimens were loaded to fracture with a loading rate of 0.5 kN/sec. Displacement vs load graphs can be seen at Figure 4.5-4.8. Titles on the graphs for K_{IIC} testing, first two letters indicate the direction of the specimen and the next number indicates the number of the test.

The same procedure in the ASTM E399 standard has been followed for the K_{IIC} calculations. The blue line on the graph indicates the tangent line to the linear region on the test data, and the red line indicates 95% slope of the tangent line. The intersection point of the test data and the 95% slope tangent line is called P_Q.

$$K_{II} = \frac{P\sqrt{\pi a}}{Wt}\left[1.006 - 0.313\left(\frac{a}{W}\right) + 3.344\left(\frac{a}{W}\right)^2 - 6.691\left(\frac{a}{W}\right)^3 + 5.649\left(\frac{a}{W}\right)^4\right]$$

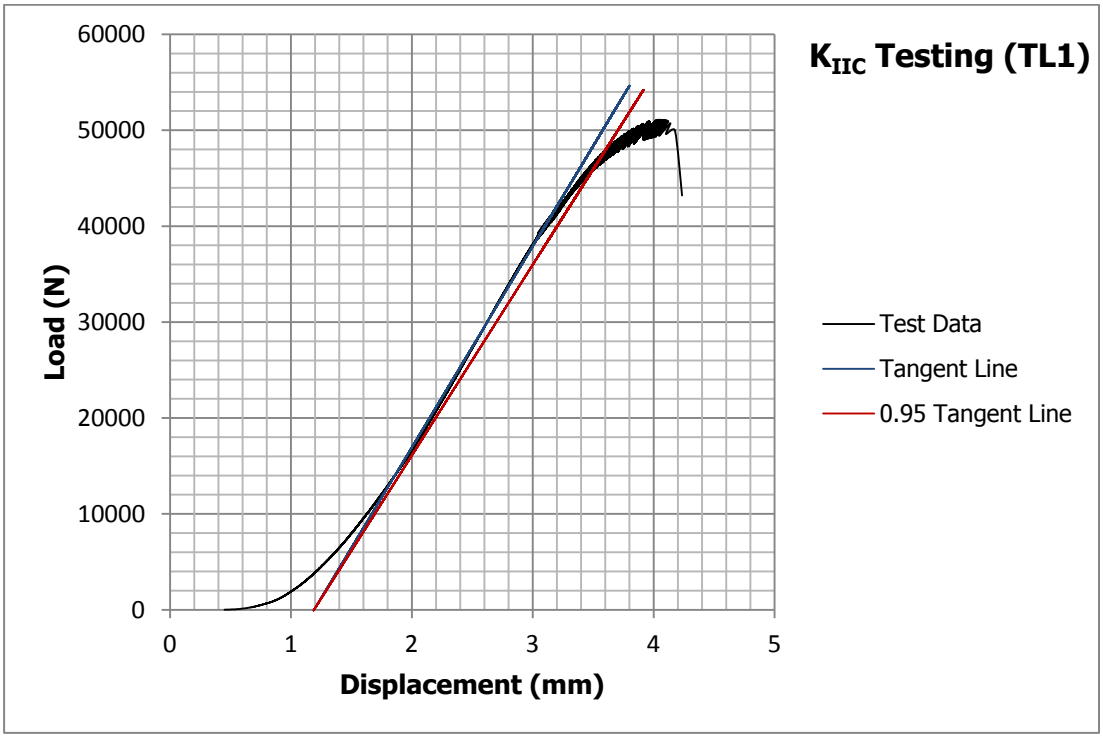

Figure 4. 5 Load vs Displacement plot for TL direction.

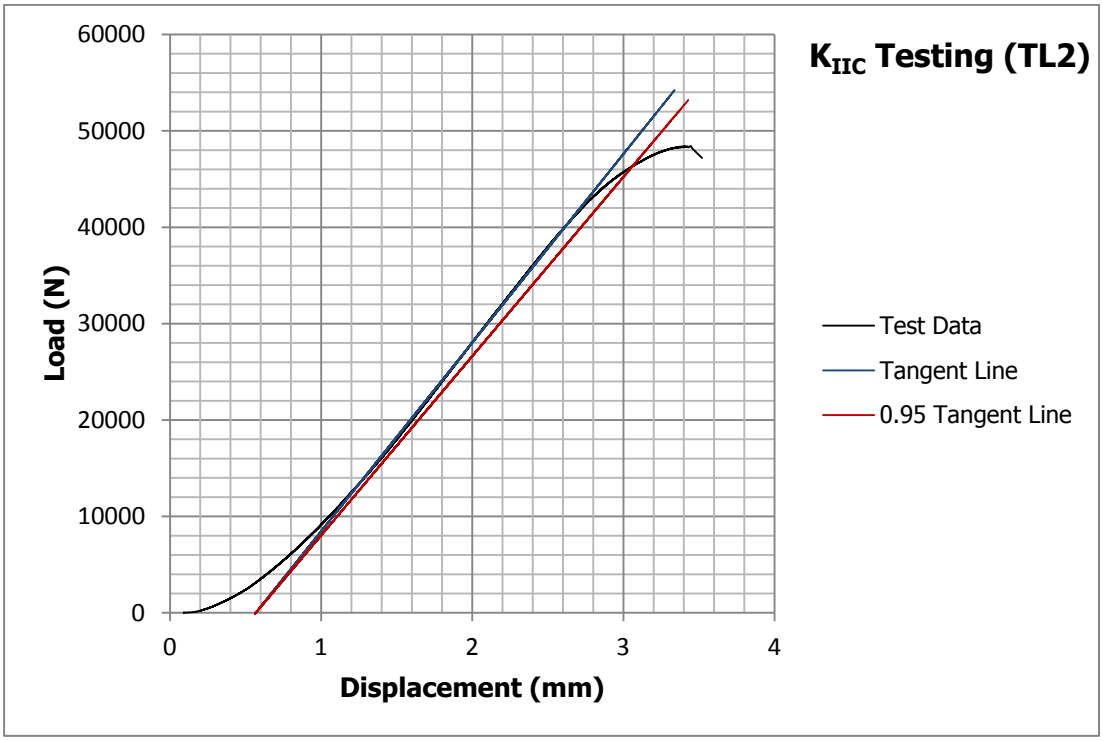

Figure 4. 6 Load vs Displacement plot for TL direction.

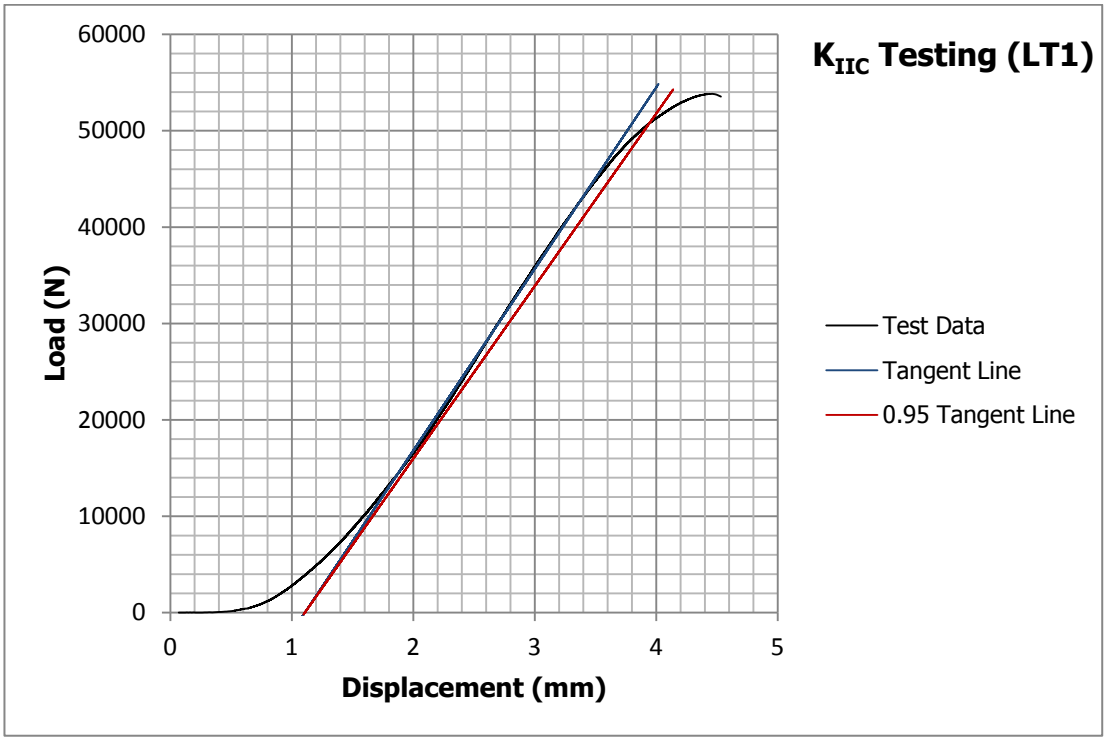

Figure 4. 7 Load vs Displacement plot for LT direction.

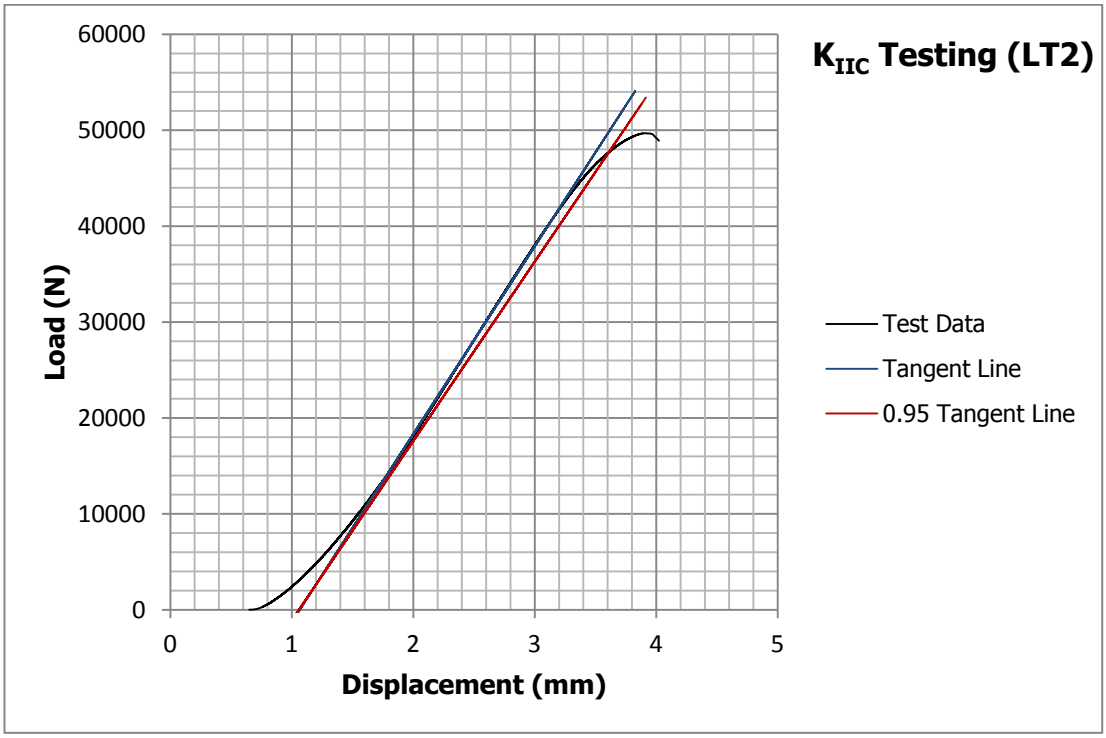

Figure 4. 8 Load vs Displacement plot for LT direction.

Required data for calculating the K_{IIC} values are tabulated in Table 4.5, and calculated K_{IIC} values compared with the K_{IC} values are given in the Table 4.6.

Table 4. 5 K_{IIC} test data.

	P_Q (N)	**a (mm)**	**W (mm)**	**t (mm)**
TL1	44255	15.5	30	10
TL2	46107	14.2	30	10
LT1	50705	14.1	30	10
LT2	47571	14.8	30	10

Table 4. 6 Comparison of K_{IC} and K_{IIC} results.

Orientation	**K_{IC} (MPa$\sqrt{m}$)**	**K_{IIc} (MPa$\sqrt{m}$)**
TL1	26.1	39.6
TL2		38.3
LT1	32.1	41.9
LT2		40.9

Ratio between K_{IIC} and K_{IC} values which were measured in this study are consistent with the literature [18, 19, 21]. In their studies, they revealed that K_{IIC} of the materials are 1.15, 1.35 and 1.5 times the corresponding K_{IC} values of the materials they used. This means that K_{IC} data can be used to predict K_{IIC} data by making approximate calculations.

Also, for both two modes of fracture toughnesses an increase in resistance to fracture is observed for LT direction.

4.3 Crack Length vs. Number of Cycle Curves

Crack length measurements were done by the travelling microscope with a resolution of ± 0.01 mm. With the collected data, crack length versus number of cycles curves were plotted. While concave up increasing curve is expected for a vs. N graphs, the cases are different from expected for the specimens TL2 and LT1. It is considered that this difference could occur because of misalignment of the loading fixture. Since crack lengths could not be measured from both sides, results from one side could not provide the requirements for the specimens except for TL3 and LT2 at all. Curves for the specimens TL1, TL2, TL3, LT1 and LT2 are shown in Figure 4.9-4.13, respectively. Equations of fitted polynomials are also given with the graphs.

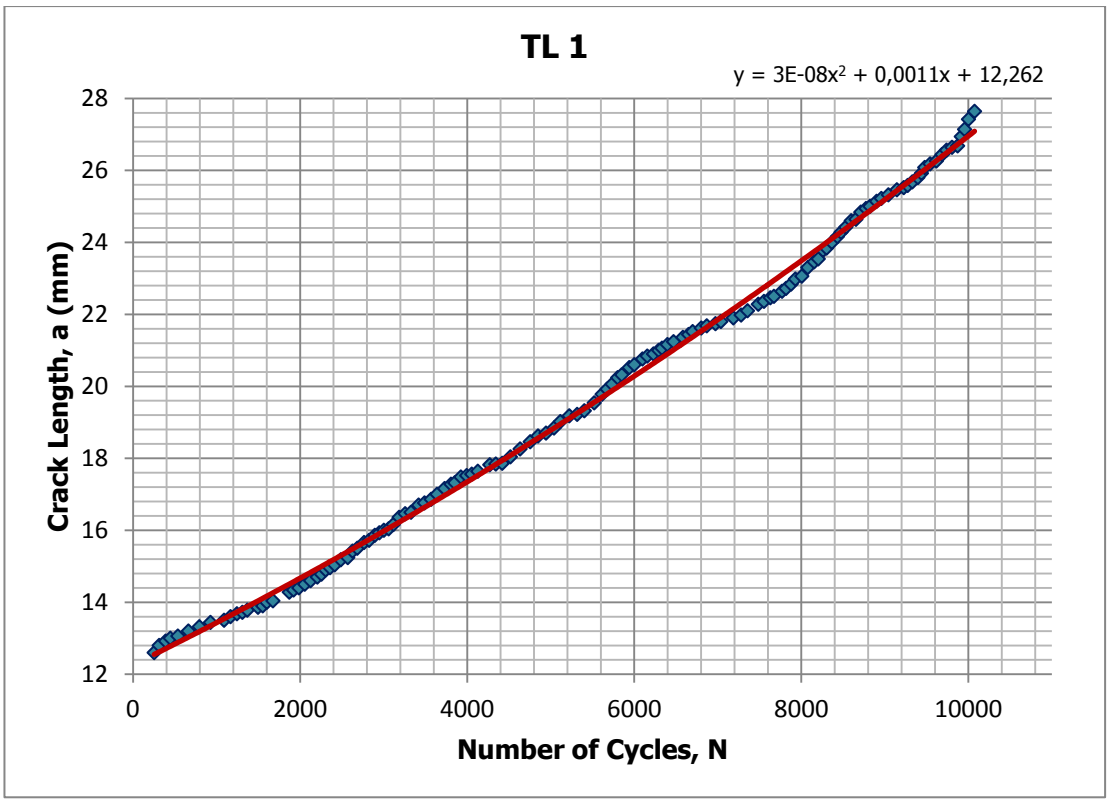

Figure 4. 9 Crack length vs. number of cycle curve for TL1 specimen.

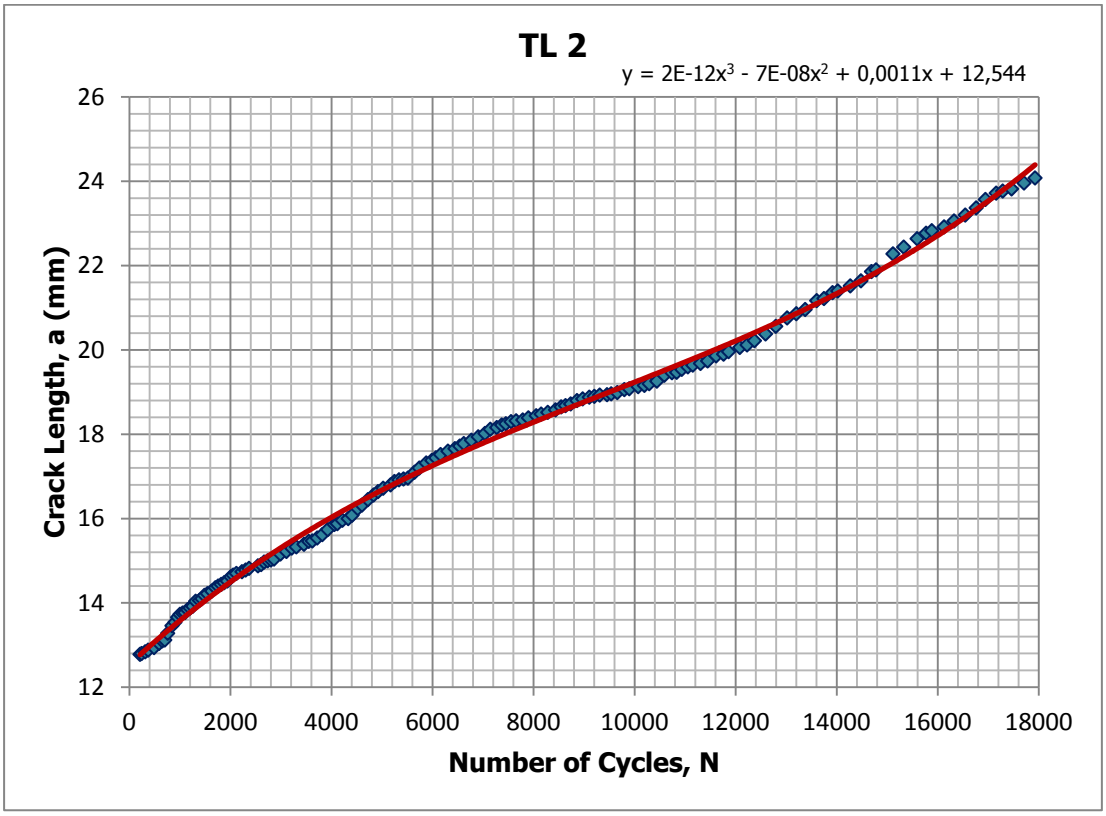

Figure 4. 10 Crack length vs. number of cycle curve for TL2 specimen.

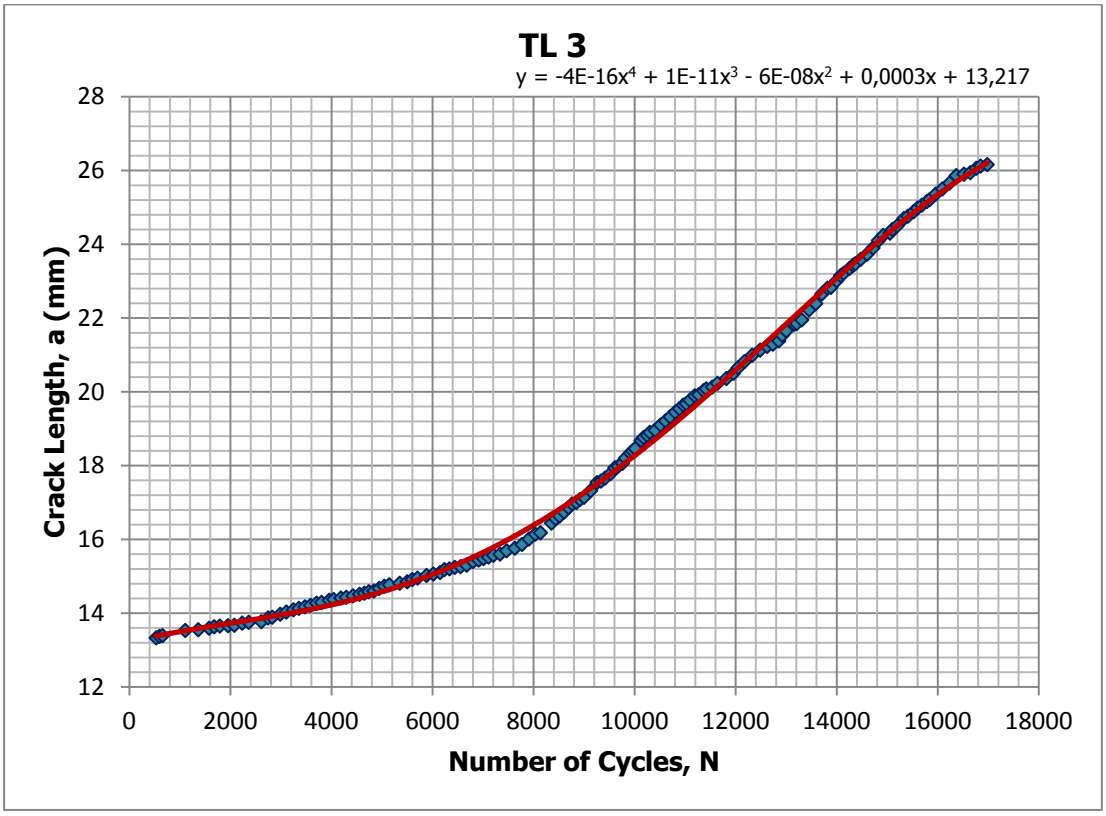

Figure 4. 11 Crack length vs. number of cycle curve for TL3 specimen.

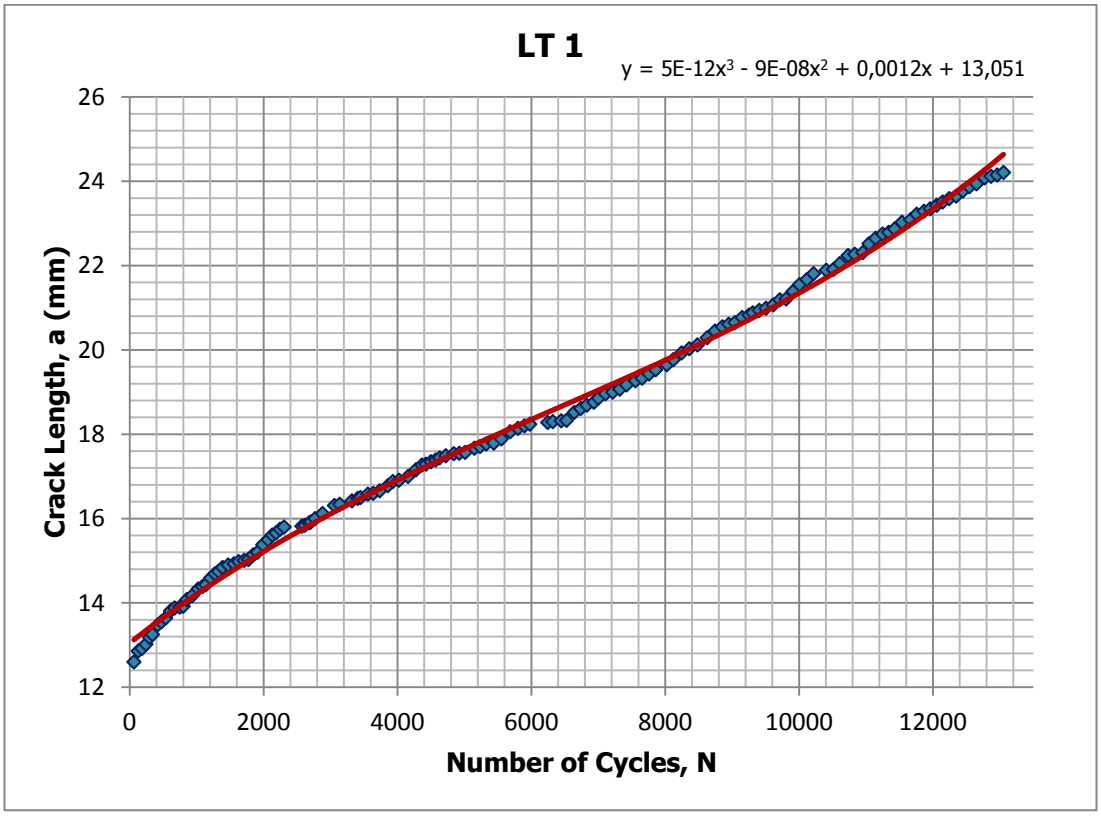

Figure 4. 12 Crack length vs. number of cycle curve for LT1 specimen.

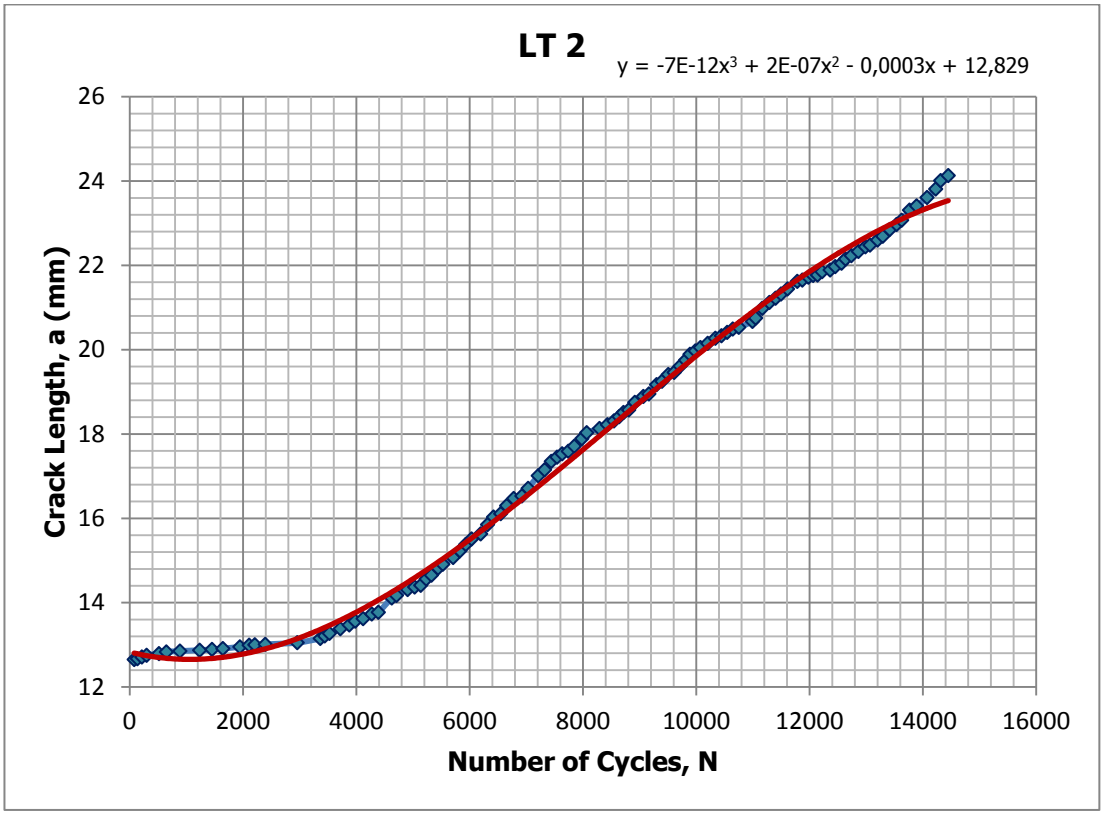

Figure 4. 13 Crack length vs. number of cycle curve for LT2 specimen.

4.4 Fatigue Crack Growth Rate versus Mode II Stress Intensity Factor Range

The fatigue crack growth rate, da/dN, data were calculated by fitting a polynomial in the second, third or fourth degree to each a vs N data. Then the derivatives of the polynomials were taken and da/dN data for each data point were calculated.

Calculated fatigue crack growth rate data with the corresponding ΔK values were plotted. Logarithmic plots of fatigue crack growth rate versus mode II stress intensity range were graphed in Figure 4.14-4.18.

Figure 4. 14 da/dN vs ΔK plot of TL1 specimen.

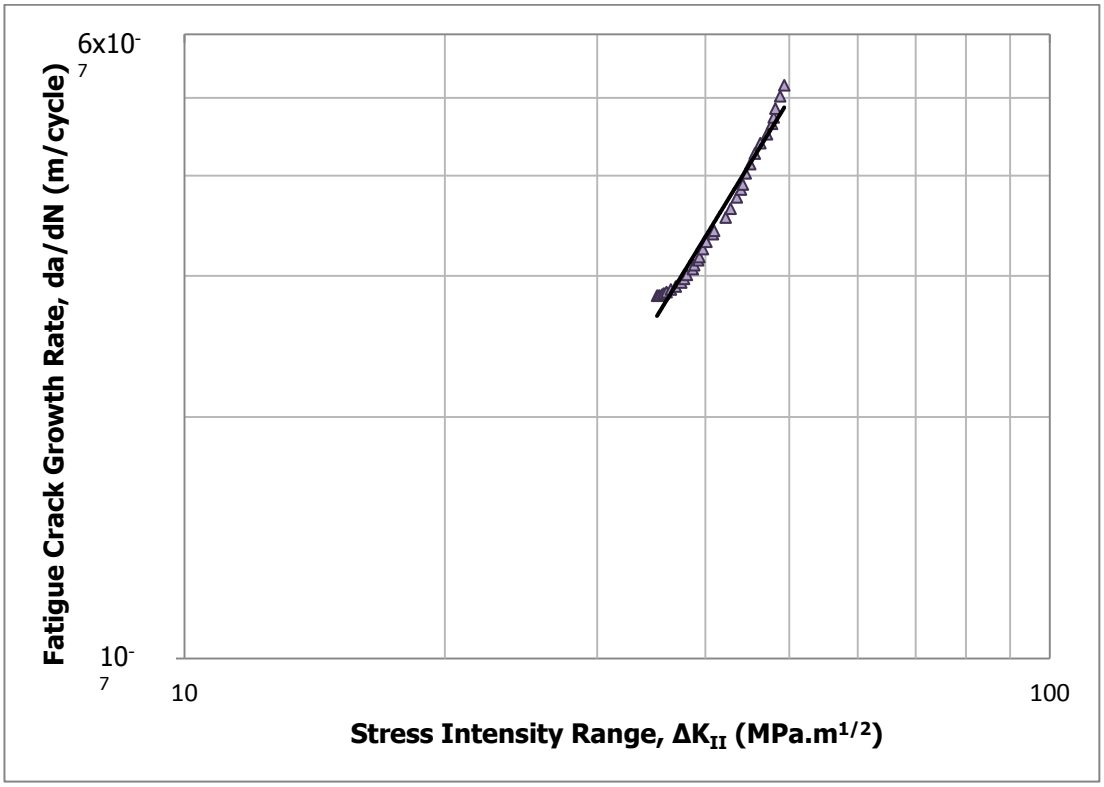

Figure 4. 15 da/dN vs ΔK plot of TL2 specimen.

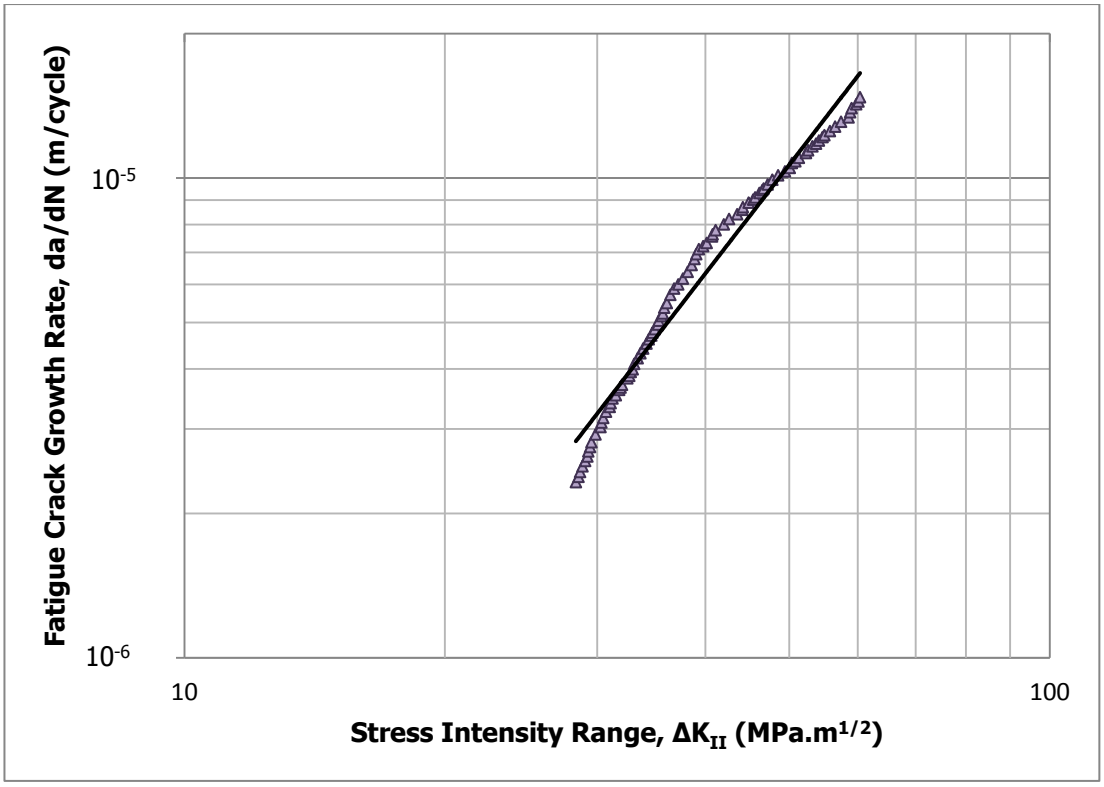

Figure 4. 16 da/dN vs ΔK plot of TL3 specimen.

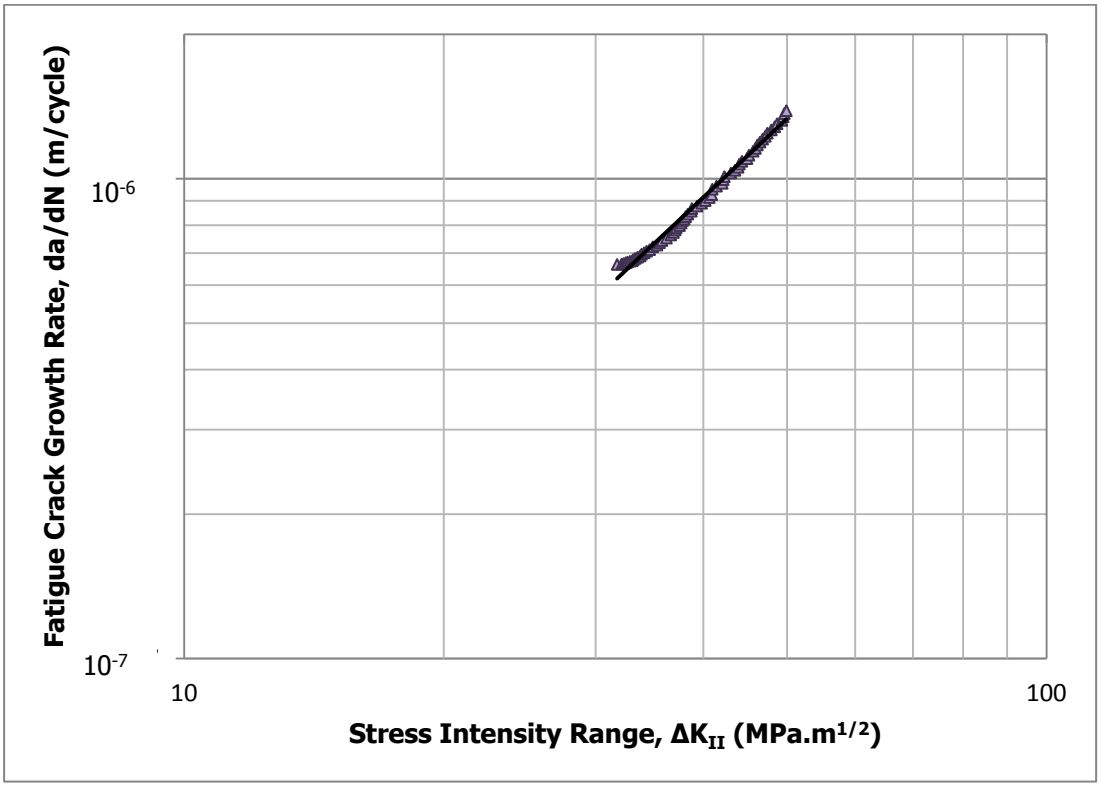

Figure 4. 17 da/dN vs ΔK plot of LT1 specimen.

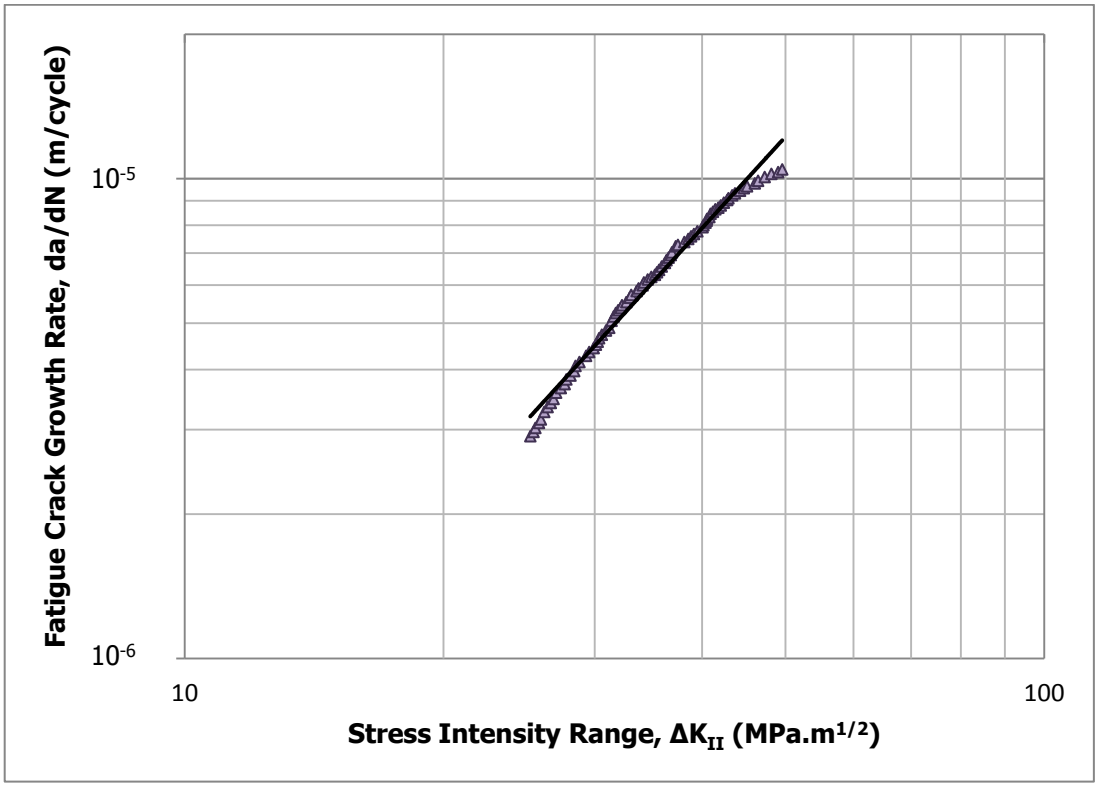

Figure 4. 18 da/dN vs ΔK plot of LT2 specimen.

4.5 Application of Paris-Erdoğan Law

To determine the constants *C* and *m* in the below Paris-Erdoğan equation, Paris-Erdoğan law was applied to stage II regions of the da/dN versus ΔK_{II} plots.

$$\frac{da}{dN} = C(\Delta K)^m$$

Curves were fitted by linear regression to the stage II regions, C and m values were calculated from the fitted power equation. Calculated C and m values and also regression values are tabulated in Table 4.7.

Table 4. 7 Constants of Paris-Erdoğan equation.

Orientation	Specimen Code	C (m/cycle)	m	R^2
TL	TL1	4×10^{-7}	0.3495	0.9630
	TL2	5×10^{-7}	1.7674	0.9731
	TL3	10^{-9}	2.3366	0.9706
LT	LT1	2×10^{-9}	1.6911	0.9911
	LT2	6×10^{-9}	1.9641	0.9855

For mode I loading, m exponent is expected to be between 2 and 4 for ductile materials [3]. TL3 specimen fits this statement, in addition to this specimen TL2 and LT2 specimens nearly conform to the statement. Regression values are high enough which means that power equations fit successfully on the stage II region and stage II regions of the plots obey the Paris-Erdoğan law.

Rates calculated for $\Delta K = 40$ MPa.$m^{1/2}$ of all specimens are shown in Table 4.8.

Table 4. 8 Mode II fatigue crack growth rate data at $\Delta K = 40$ MPa.$m^{1/2}$.

Orientation	Specimen Code	da/dN(m/cycle)	Stress Ratio (R)
TL	TL1	1.452×10^{-6}	-1
	TL2	3.391×10^{-4}	-1
	TL3	5.538×10^{-6}	-1
LT	LT1	1.023×10^{-6}	-1
	LT2	8.409×10^{-6}	-1

The rates for mode II fatigue crack growth seems not consistent in each orientation group, but for TL3 and LT2 specimens, as their crack length versus cycle plots are more proper than the others, calculated rate data for them are more reliable than the others. The specimen in TL orientation shows the highest fatigue crack growth resistance as can be seen from Figure 4.19. A large difference in second phase distribution was not observed in both orientations, but there is a slight difference in rates.

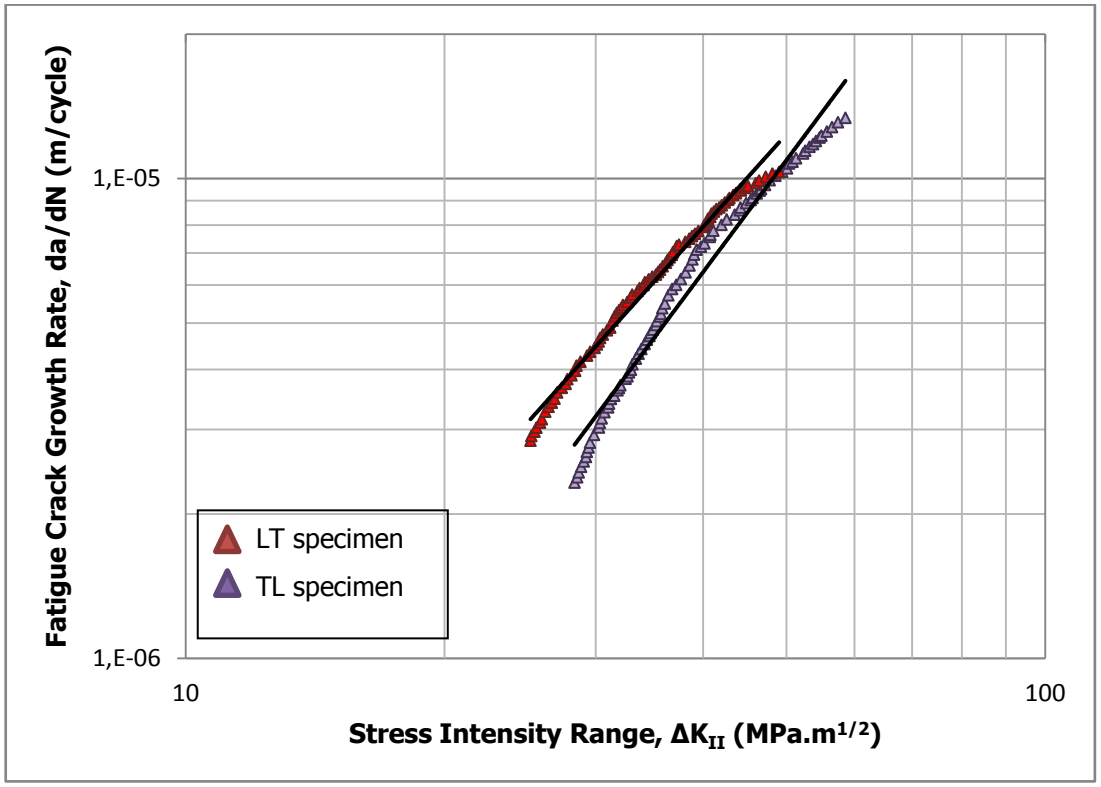

Figure 4. 19 da/dN vs ΔK plot of TL3 and LT2 specimen.

In other studies [43, 44], C and m constants were obtained for the same material for mode I type of loading. Data for C and m constants and corresponding fatigue crack growth rates at $\Delta K = 40$ MPa.m$^{1/2}$ are given in Table 4.9.

Table 4. 9 C and m constants measured in other mode I fatigue crack growth studies.

Specimen	C (m/cycle)	m	da/dN at ΔK = 40 MPa.m$^{1/2}$	Stress Ratio (R)
Specimen [43]	2×10^{-9}	1.85	1.840×10^{-6}	0.1
TL Specimen [44]	1.12×10^{-12}	3.48	4.211×10^{-7}	0.1
LT Specimen [44]	1.86×10^{-9}	2.94	9.540×10^{-5}	0.1

As seen from the Tables 4.8 and 4.9, TL specimen on the Table 4.9 is more resistant than that of all mode II specimens in TL orientation; fatigue crack growth rate under mode II loading is higher in TL orientation. Also, mode II specimens in LT orientation are more resistant than that of LT specimen shown on Table 4.9; fatigue crack growth rate under mode I loading is higher in LT orientation. For the specimen on the Table 4.9 without a designation, the value is closer to TL1 and LT1 specimens, but the rate of it is lower than TL3 and LT2 specimens, which are more reliable in this study. As a result, the values are somewhat equal to each other.

It was observed in other studies [45] that for the same ΔK values, crack growth rate increases with decreasing stress ratios; namely, rate in -1 stress ratio is lower than the rate in 0.1 stress ratio for the same ΔK value. Since the stress ratios are different in mode I studies, it can be thought that mode I fatigue crack growth rates would be higher if they would have been done as their stress ratios are -1.

Improper results in each orientation groups obtained in this study for fatigue crack growth rates are simply because of the test conditions. Taking data from both surfaces and adjusting the loading fixture of testing machine's alignment properly would make the results more reliable and consistent with each other.

4.6 Macro Examination of the Fracture Surfaces

After mode II fracture toughness tests and mode II fatigue crack growth tests, macro photographs were taken. Figures 4.20-4.21 show the fracture surfaces of some of the specimens.

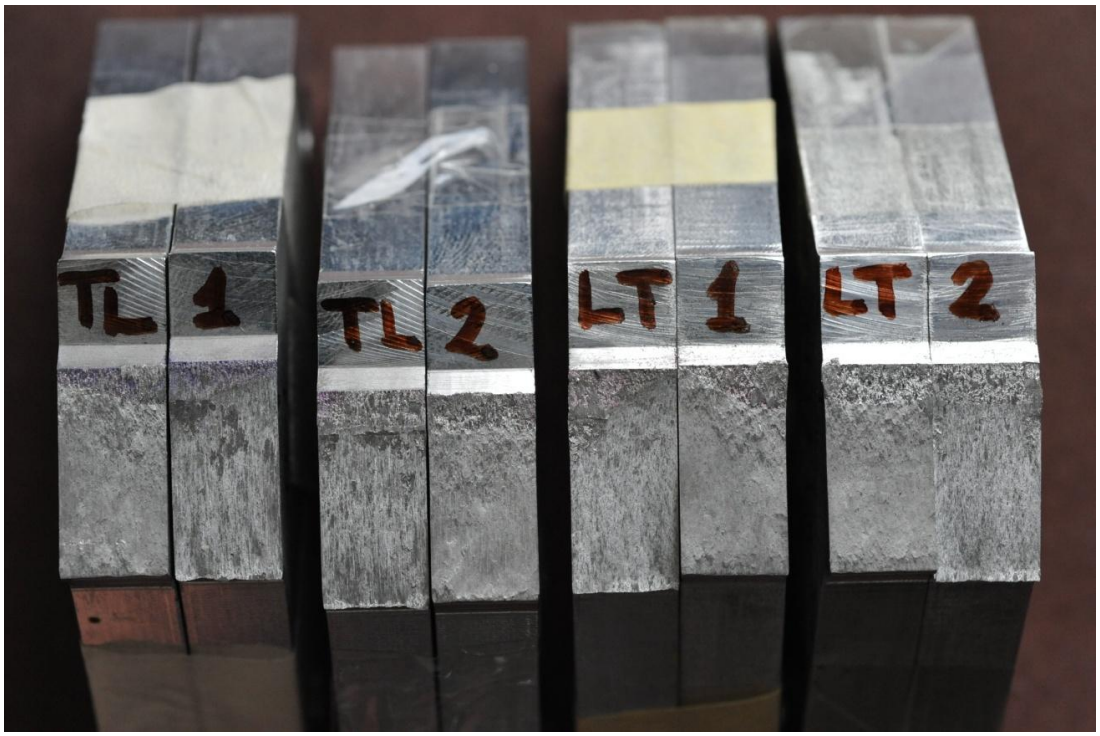

Figure 4. 20 Fracture surfaces of mode II fracture toughness specimens.

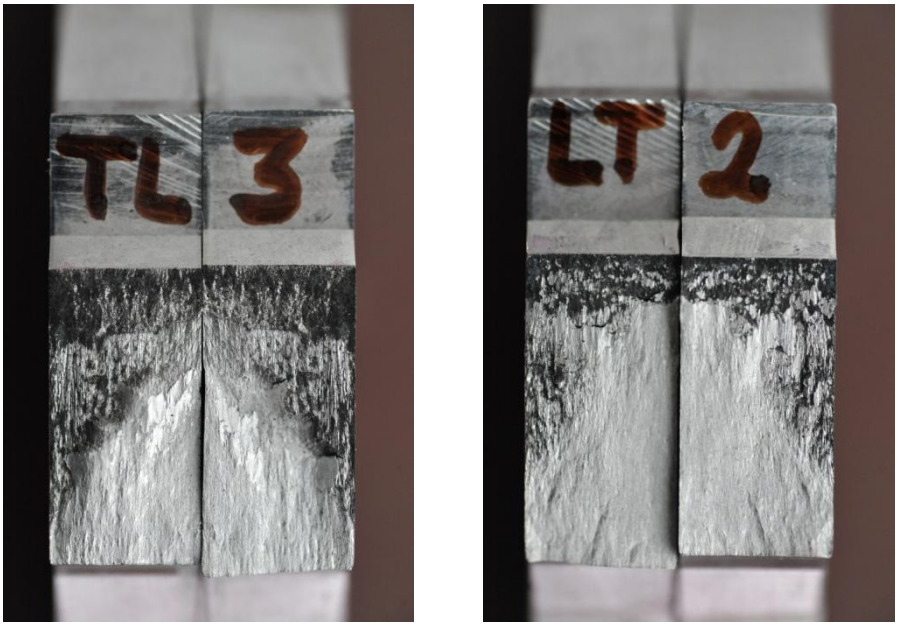

Figure 4. 21 Fracture surfaces of mode II fatigue crack growth specimens.

4.7 SEM Examination of the Fracture Surfaces

Fractographs taken by scanning electron microscope (SEM) are given in Figures 4.22-4.39. The aim in examining the fracture surfaces by SEM was to reveal the characteristics of the fracture and fatigue crack growth under mode II loading condition. A white arrow on the fractographs shows the crack growth direction.

Also, energy dispersive spectrum (EDS) analyses were performed to analyze the composition of second phase particles.

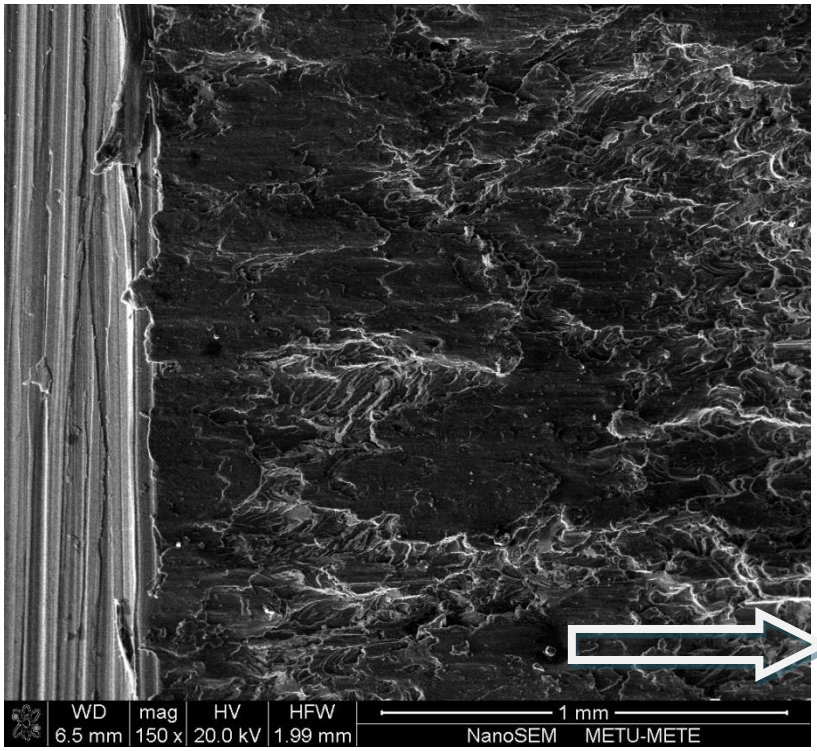

Figure 4. 22 Beginning of precrack region (LT direction - K_{IIC} specimen).

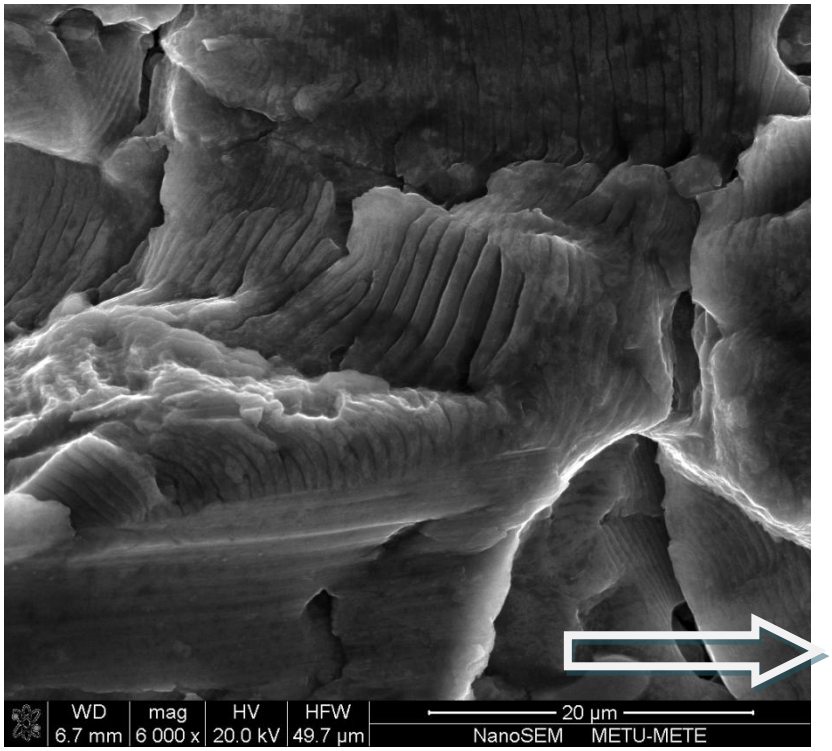

Figure 4. 23 Fatigue striations on tear ridges in the precrack region (LT direction - K_{IIC} specimen).

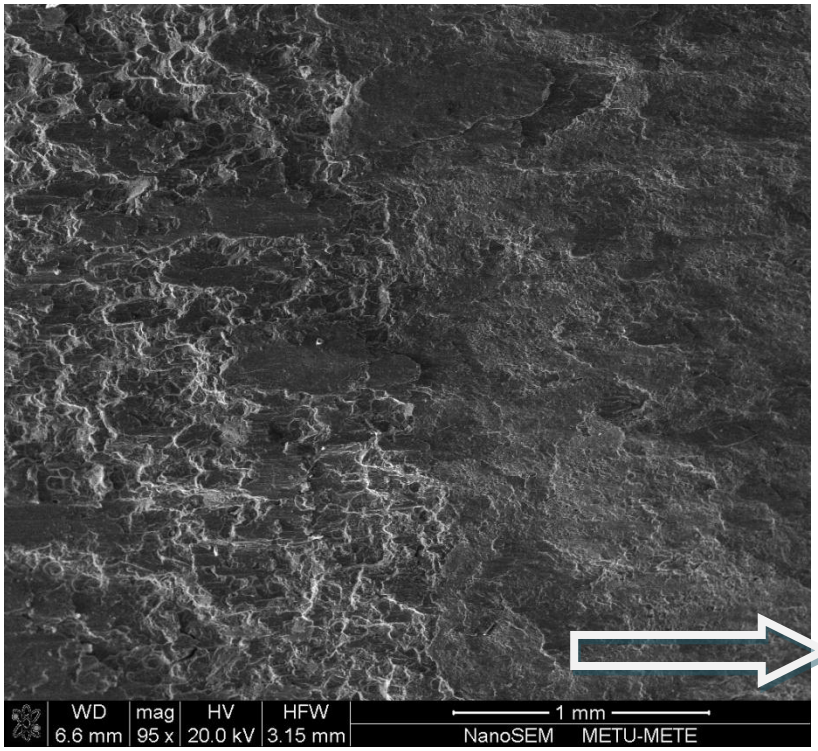

Figure 4. 24 Transition from precrack region to unstable crack growth region (LT direction – K_{IIC} specimen).

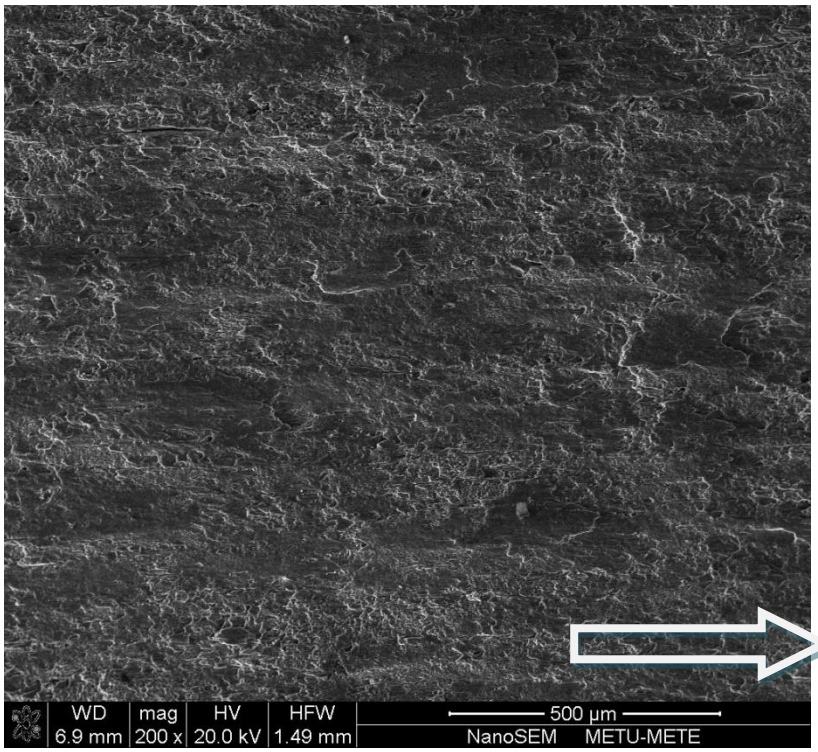

Figure 4. 25 General view of the fracture surface (LT direction - K_{IIC} specimen).

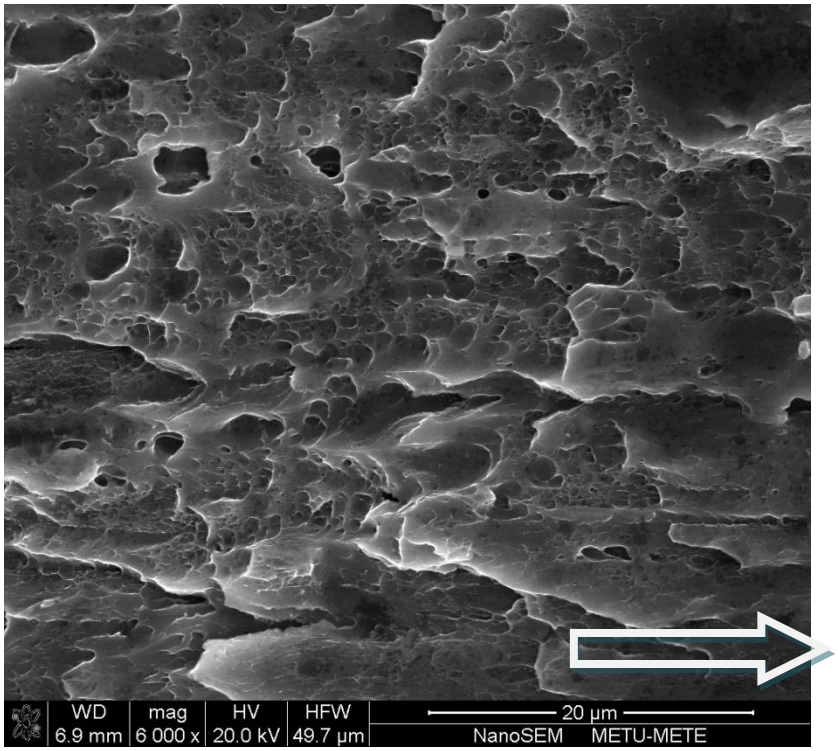

Figure 4. 26 Sudden fracture region (LT direction - K_{IIC} specimen).

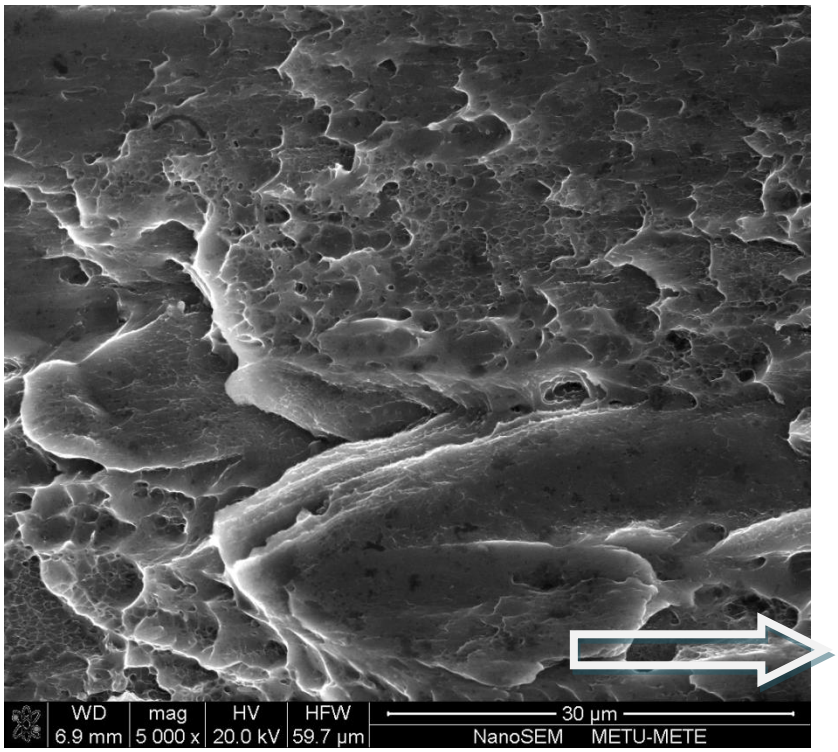

Figure 4. 27 Sudden fracture region (LT direction - K_{IIC} specimen).

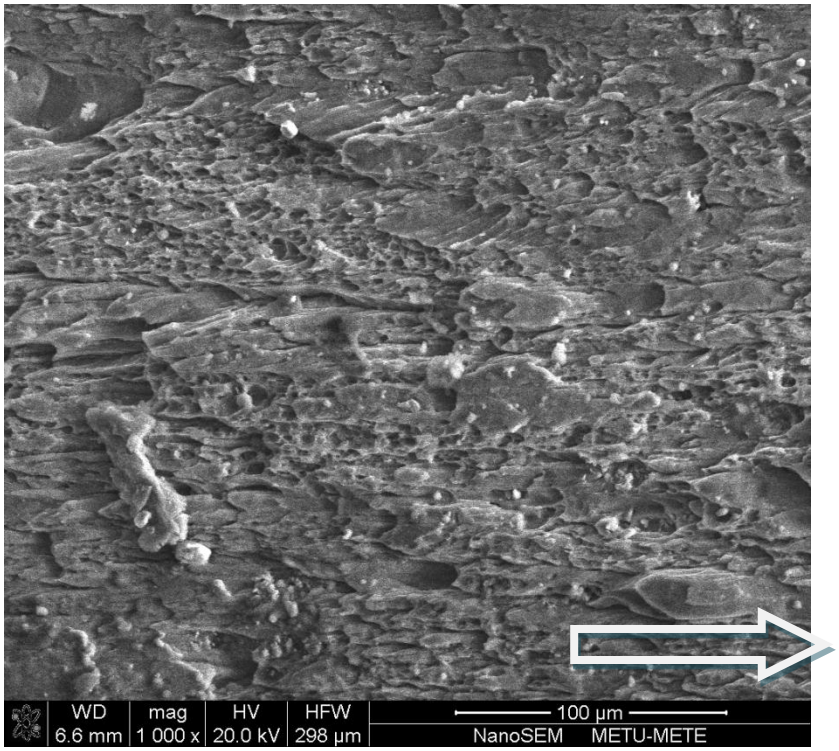

Figure 4. 28 General view of the sudden fracture surface (TL direction - K_{IIC} specimen).

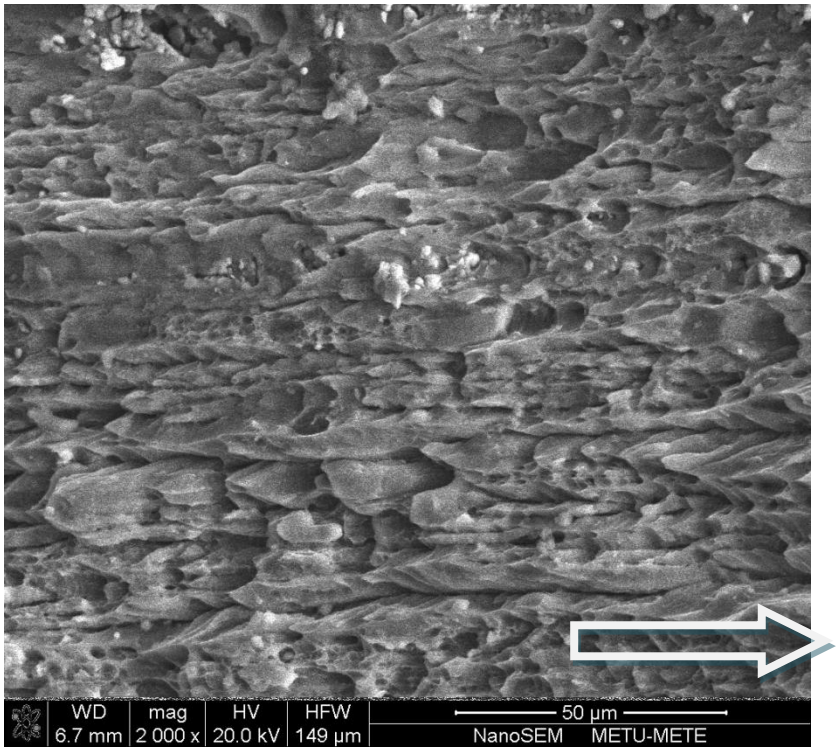

Figure 4. 29 Sudden fracture surface (TL direction - K_{IIC} specimen).

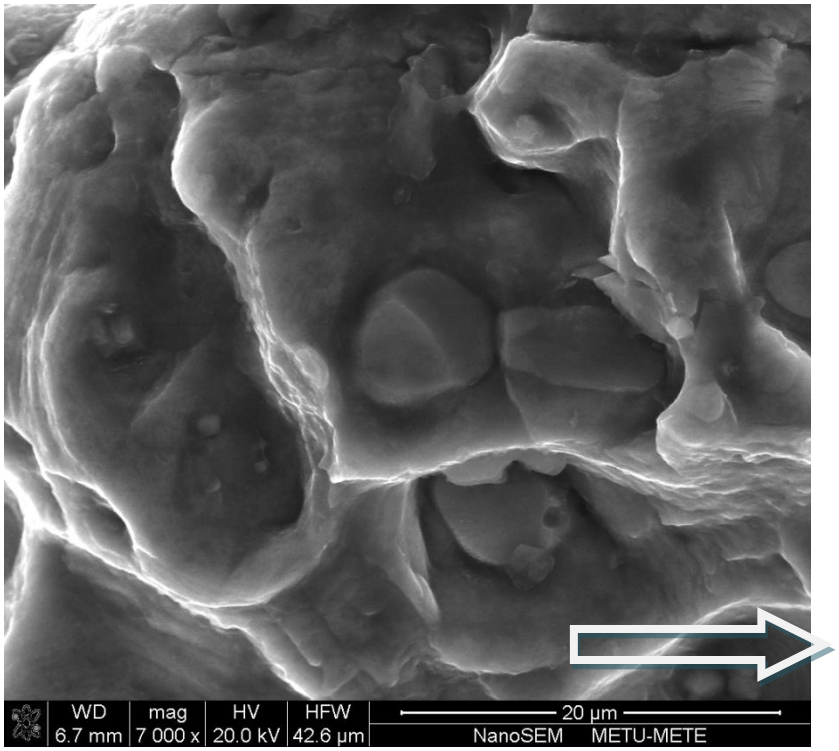

Figure 4. 30 A second phase particle ($CuAl_2Mg$) in a void in the precrack region (LT direction - K_{IIC} specimen).

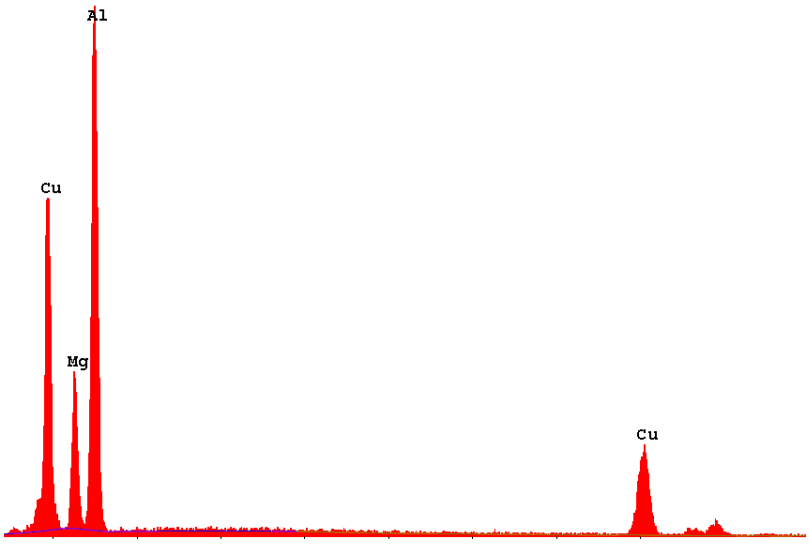

Figure 4. 31 EDS of the particle in Figure 4.29.

There are striations observed in the precrack region of mode II fracture toughness specimens (Fig.4.22). Also secondary cracks are observed. Dimples in the shear region are different from mode I fatigue dimples. Because of shear type of loading, dimples and voids are elongated and elongated voids can be seen in Figures 4.26 - 4.29.

From the EDS and the fractograph of a second phase particle shown in Figure 4.30, this spherical particle can be classified as $CuAl_2Mg$, as reported by Mondolfo [30].

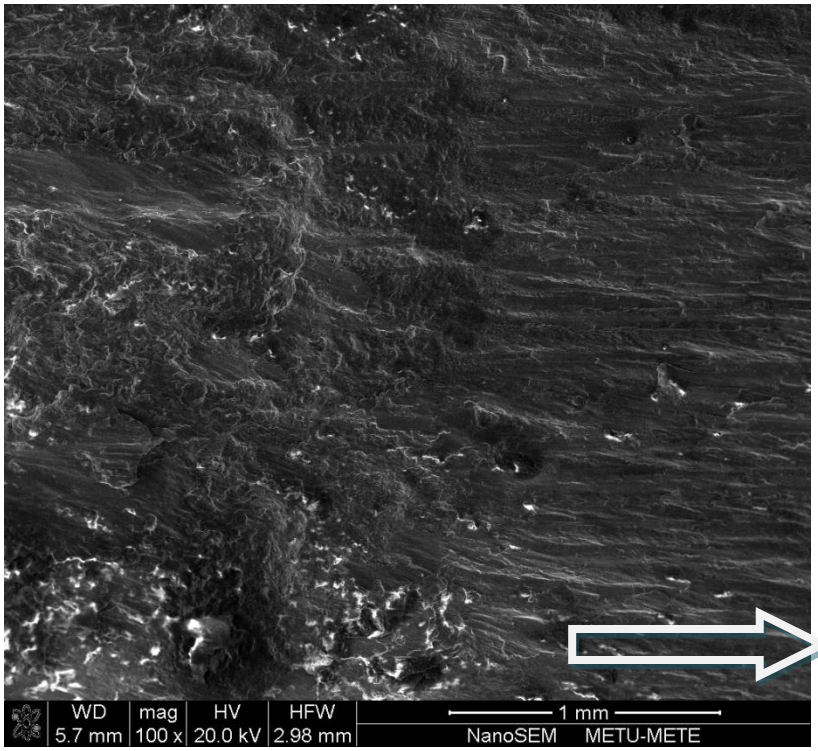

Figure 4. 32 Transition from precrack region to mode II fatigue crack growth region (TL direction – Mode II FCGR specimen).

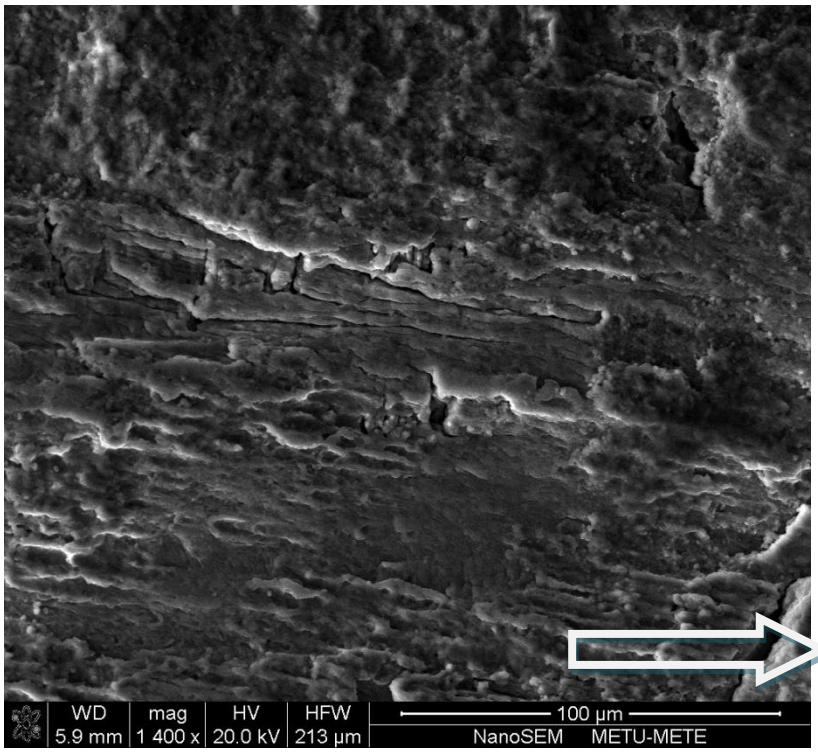

Figure 4. 33 Secondary cracks in mixed ways (TL specimen - Mode II FCGR specimen).

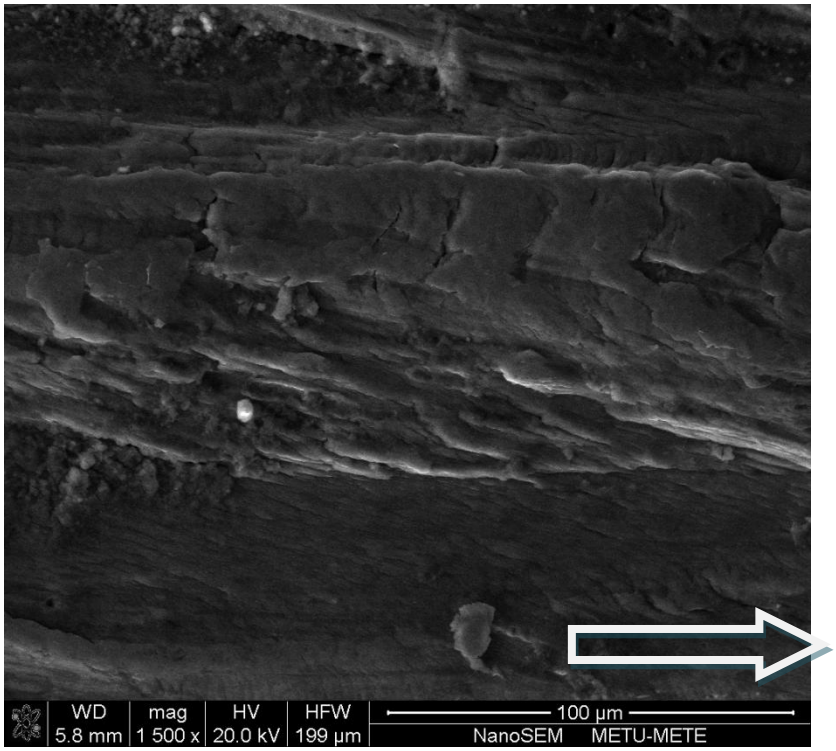

Figure 4. 34 Striations and secondary cracks, plastered tear ridges (TL specimen - Mode II FCGR specimen).

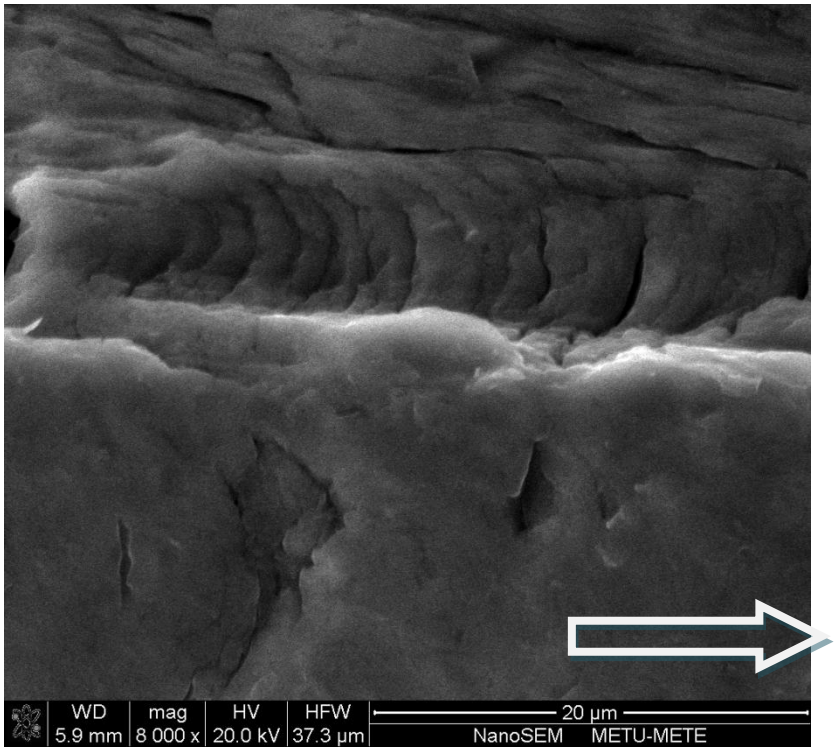

Figure 4. 35 Striations (TL specimen - Mode II FCGR specimen).

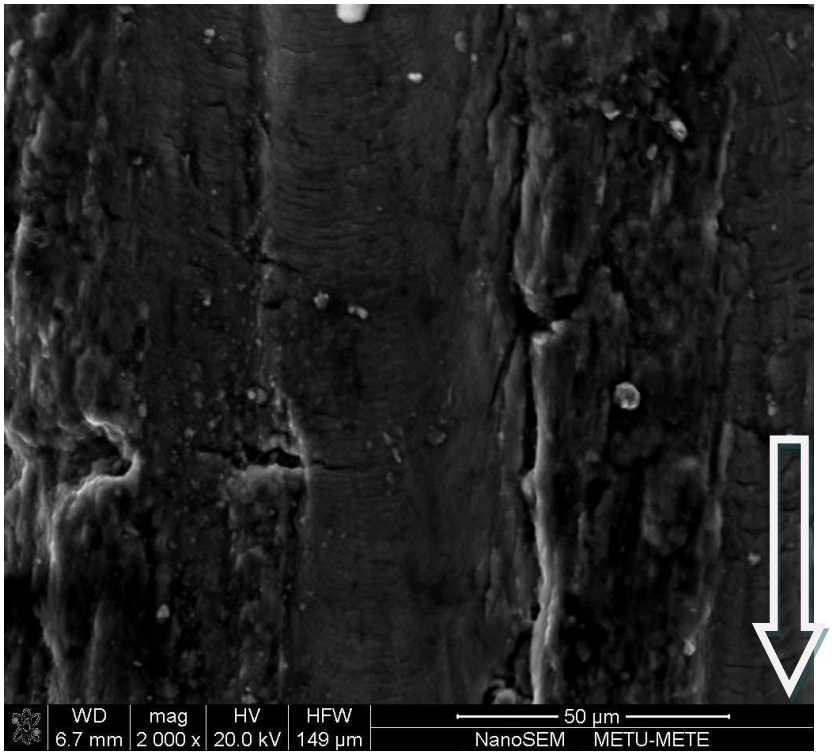

Figure 4. 36 Striations and deformation (TL specimen - Mode II FCGR specimen).

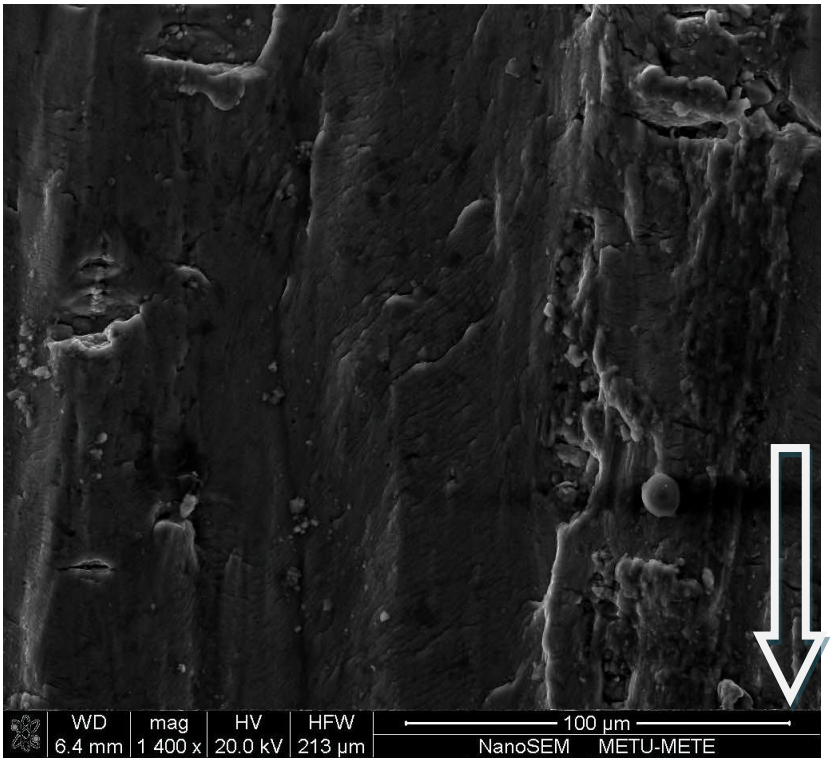

Figure 4. 37 Striations and deformation (TL specimen - Mode II FCGR specimen).

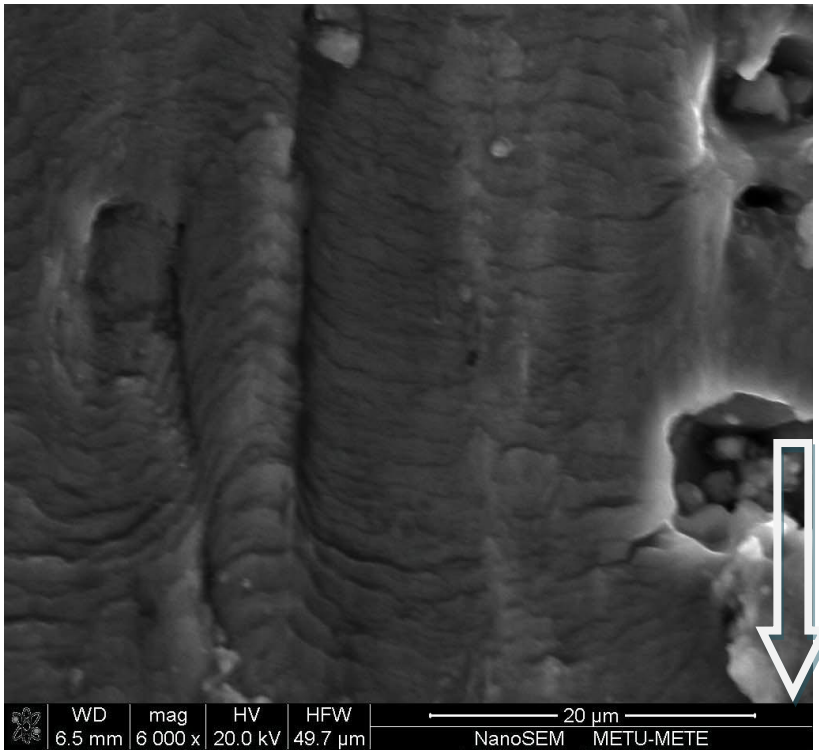

Figure 4. 38 Tear ridges with striations, second phase particles in voids (TL specimen Mode II FCGR specimen).

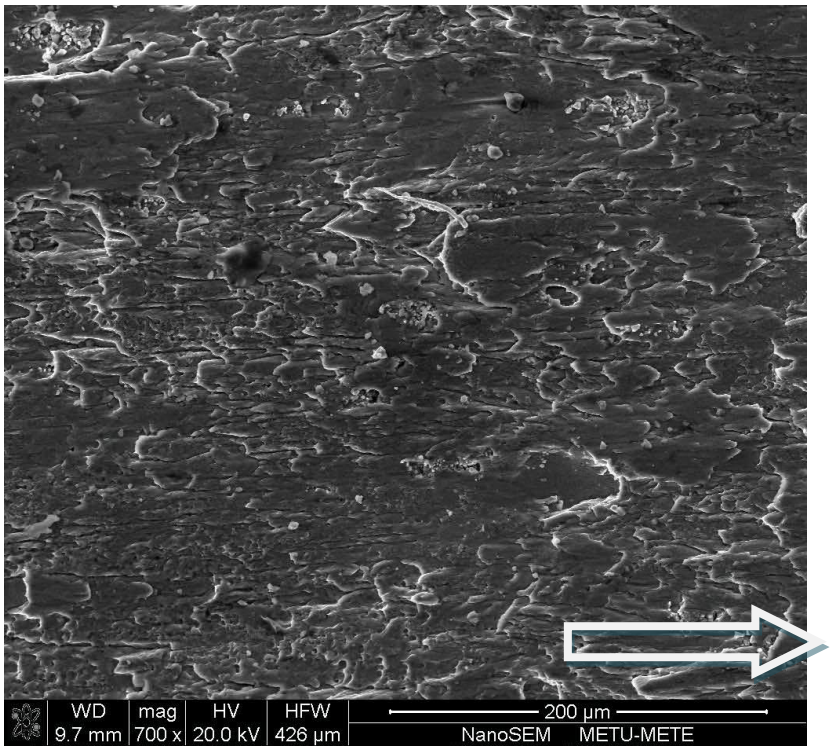

Figure 4. 39 General view of fatigue crack growth region (LT specimen - Mode II FCGR specimen).

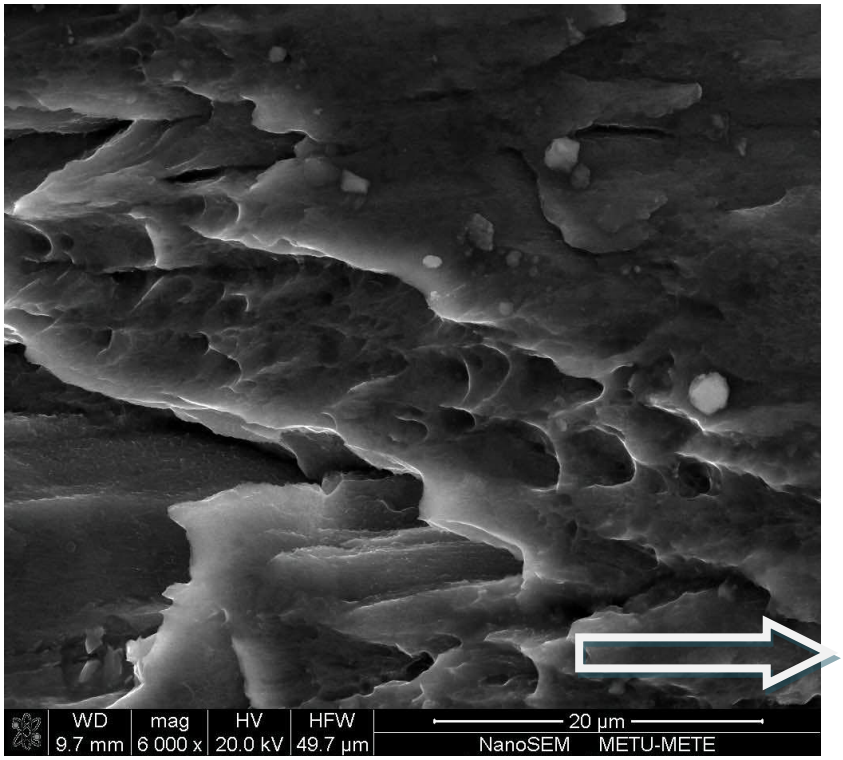

Figure 4. 40 Elongated dimples due to fast fracture (LT specimen - Mode II FCGR specimen).

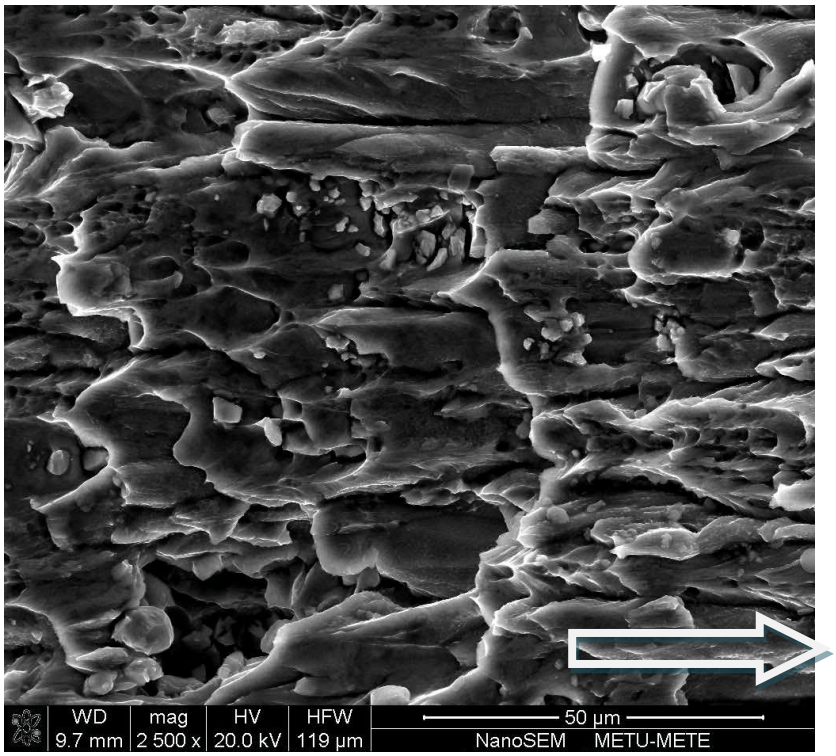

Figure 4. 41 Fast and unstable crack growth (LT specimen - Mode II FCGR specimen).

A large amount of deformation caused by rubbing can be seen on the fracture surfaces. Secondary cracks are also observed.

4.8 Visualization of Shear Concentration on FEM Model

It was assumed that the specimen was fixed from the three holes on the right hand side and 15000N force was applied downwards and upwards from the holes on the left hand side. The scale on the right side shows the magnitude of the stress concentration. According to this scale, there exists nearly 640 MPa stress concentration on the crack tip when 15000N force applied.

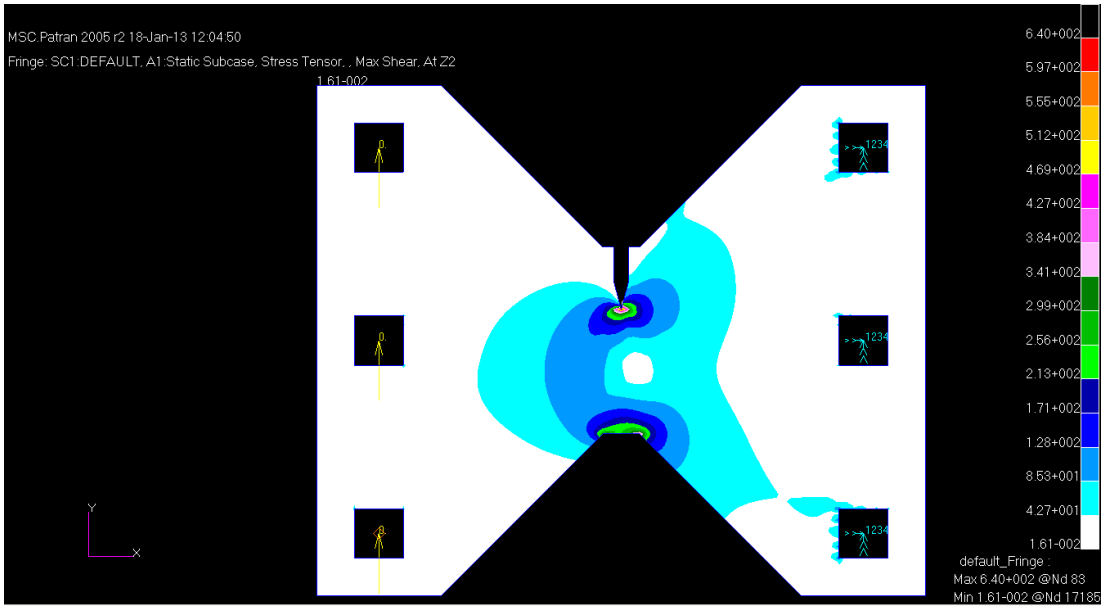

Figure 4. 42 Shear concentration on the specimen.

CHAPTER 5

CONCLUSIONS

The aim of this study was to calculate the mode II fracture toughness values and to investigate mode II fatigue crack growth behavior of AA7050-T7451 alloy in two orientations.

From the results of the mode II fracture toughness and mode II fatigue crack growth rate tests, following conclusions may be drawn:

1. Measured K_{IIC} values are 1.3 between 1.5 times of the K_{IC} values, which means the results are consistent with the literature.

2. K_{IIC} values in the LT directions are higher than those of TL directions.

3. The specimen in TL orientation shows the highest mode II fatigue crack growth resistance.

4. The design and geometry of the specimen and the loading frame can be used in further studies for measuring K_{IIC} values and mode II fatigue crack growth rates since the FEM analysis show that shear stress concentrates on the crack tip.

REFERENCES

[1] L.Banks-Sills, M.Arcan, "A Compact Mode II Fracture Specimen", Fracture Mechanics, Vol.17, 347-363, (1986)
[2] M.Janssen, J.Zuidema, and R.Wanhill, "Fracture Mechanics", Spon Press, (2002)
[3] S.Suresh, "Fatigue of Materials", Cambridge University Press, (1996)
[4] http://www.keytometals.com/page.aspx?ID=CheckArticle&site=kts&NM=299
[5] R.W.Hertzberg, "Deformation and Fracture Mechanics of Engineering Materials", Wiley, (1996)
[6] W.A. Wood, Bull. Inst. Met., Vol.3, 5-6, (1955)
[7] G.E.Dieter, "Mechanical Metallurgy", McGraw Hill, (1988)
[8] C.Laird and G.C.Smith, "Initial Stages of Damage in High Stress Fatigue in Some Pure Metals", Philosophical Magazine, Vol.8, 1945-1963, (1963)
[9] W.D.Callister, "Fundamentals of Materials Science and Engineering", Wiley, (2001)
[10] ASM Handbook, "Fatigue and Fracture", Vol.19, ASM, (2000)
[11] P.C.Paris and F.Erdoğan, "A Critical Analysis of Crack Propagation Laws", Trans. ASME, J.Basic Eng., Vol.85, 528-534, (1963)
[12] R.G.Forman, V.E.Kearney, and R.M.Engle, "Numerical Analysis of Crack Propagation in Cyclic Load Structure", Trans.ASME, J.Basic Eng., Vol.89, 459, (1967)
[13] D.Broek, "Elementary Engineering Fracture Mechanics", Kluwer Academic Publishers, (1986)
[14] R.A.Pearson, Engineering Fracture Mechanics, Vol.7, 235-247, (1972)
[15] H.LEwalds and R.J.H.Wanhill, Fracture Mechanics, Edward Arnold, (1984)
[16] ASTM E1823-09a, Standard Terminology Relating to Fatigue and Fracture Testing
[17] A.A.Merati et al, "On The Mixed Mode II/III Fatigue Threshold Behaviour For Aluminium Alloys 2014-T6 and 7075-T6", Fatigue & Fracture of Engineering Materials & Structures, Vol.34(11), doi:10.1111/j.1460-2695.2011.01560.x, (2011)
[18] D.L.Jones, and D.B.Chisholm, "An Investigation of the Edge-Sliding Mode in Fracture Mechanics", Engineering Fracture Mechanics, Vol. 7, 261-270 (1975)
[19] W.Hiese and J.E.Kalthoff, "Recommendations for the Determination of Valid Mode II Fracture Toughnesses K_{IIC}", Mixed-Mode Crack Behavior, ASTM STP 1359, Society for Testing and Materials, (1999)
[20] N.Tsangarakis, "Mode II Fracture Toughness of 4340 Steel", Engineering Fracture Mechanics, Vol.22(4), 617-624, (1985)
[21] N.Tsangarakis, "All Modes FractureToughness of Two Aluminum Alloys", Engineering Fracture Mechanics, Vol. 26(3), 313-321, (1987)
[22] R.J.Buzzard, B.Gross, J.E.Srawley, "Mode II Fatigue Crack Growth Specimen Development", Fracture Mechanics, Vol.17, 329-346, (1986)
[23] Y.Murakami and S.Hamada, "A New Method for the Measurement of Mode II Fatigue Threshold Stress Intensity Factor Range ΔK_{IIth}", Fatigue Fract. Engng Mater. Struct., Vol. 20(6), 863-870, (1997)
[24] A.Otsuka, Y.Fujii, and K.Maeda, "A New Testing Method to Obtain Mode II Fatigue Crack Growth Characteristics of Hard Materials", Fatigue & Fracture of Engineering Materials & Structures, Vol. 27(3), 203–212, (2004)
[25] M.O.Wang, R.H.Hu, C.F.Qian and J.C.M.Li, "Fatigue Crack Growth Under Mode II Loading", Fatigue & Fracture of Engineering Materials & Structures, Vol.18, 1443–1454, doi: 10.1111/j.1460-2695.1995.tb00867.x, (1995)
[26] A.Otsuka, H.Sugawara and M.Shomura, "Test Method For Mode II Fatigue Crack Growth Relating To A Model For Rolling Contact Fatigue", Fatigue & Fracture of Engineering Materials & Structures, Vol.19, 1265-1275, doi: 10.1111/j.1460-2695.1996.tb00949.x, (1996)

[27] K.Makoto and O.Takeshi, "Evaluation of Mode II Fatigue Crack Growth and Fractography, Journal Code: L0191A, Vol.1999, 567-568, (1999)
[28] Robert P.Wei, "Fracture Mechanics – Integration of Mechanics, Material Science, and Chemistry", Cambridge University Press, (2010)
[29] J.J.Schubbe, "Plate Thickness Variation Effects on Crack Growth Rates in 7050-T7451 Alloy Thick Plate", Journal of Materials Engineering and Performance, Vol. 20(1), (2011)
[30] L.F.Mondolfo, "Al Alloys: Structure and Properties", Butterworths, (1976)
[31] Handbook of Aluminum, Marcel Dekker, (2003)
[32] F.Y.Xie, X.Y.Yan, L.DIing, F.Zhang, S.L.Chen, M.G.Chu, A.Y.Chang, "A Study of Microstructure and Microsegregation of Aluminum 7050 alloy", Mate Sci Eng A, Vol.335, 144−153, (2003)
[33] L.L.Rokhlin, T.V.Dobatkina, N.R.Bochvar, E.V.Lysova, "Investigation of Phase Equilibria in Alloys of Al-Zn-Mg-Cu-Zr-Sc System", Journal of Alloys and Compounds, Vol.367, 10-16, (2004)
[34] X.M.Li, M.J.Starink, "Effect of Compositional Variations on Characteristics of Coarse Intermetallic Particles in Overaged 7000 Aluminium Alloys, Mate Sci Tech, Vol.17, 1324−1328, (2001)
[35] R.Gurbuz, S.P.Alpay, "The Effect of Coarse Second Phase Particles on Fatigue Crack Propagation, Scripta Metallurgica et Materialia, Vol.30(11), 1373−1376, (1994)
[36]J.E.Hatch, "Aluminum Properties and Physical Metallurgy", ASM International, (1984)
[37] C.L.Briand, "Mechanical Aspects of Environmental Failures", 181, Elsevier, (1985)
[38] ASM Speciality Handbook, Al and Al Alloys, Heat Treating of Al Alloys, 675-718, (1993)
[39] EN 10002-1, Tensile Testing of Metallic Materials. Method of Test at Ambient Temperature
[40] ASTM E384 - 11e1, Standard Test Method for Knoop and Vickers Hardness of Materials
[41] ASTM E23-07ae1, Standard Test Methods for Notched Bar Impact Testing of Metallic Materials
[42] ASTM E399 – 09e2, Standard Test Method for Linear-Elastic Plane-Strain Fracture Toughness K_{IC} of Metallic Materials
[43] N.Akgun, "Effect of Retrogession and Reaging Heat Treatment on Corrosion Fatigue Crack Growth Behavior of AA7050 Alloy", METU, (2004)
[44] R.Gurbuz, M.Doruk and W.Schutz, "Effect of Salt-Water Fog on Fatigue Crack-Growth Behavior of 7050-Aluminum Alloy in Different Orientations", J Mater Sci, Vol.26(4), 1032-1038, (1991)
[45] C.M.Hudson, "Effect of Stress Ratio on Fatigue-Crack Growth in 7075-T6 and 2024-T3 Aluminum Alloy Specimens", Langley Research Center, NASA TN D-5390, (1969)